The RAGazine

Volume 3 Issue 2-3 February 2016

Double Issue!

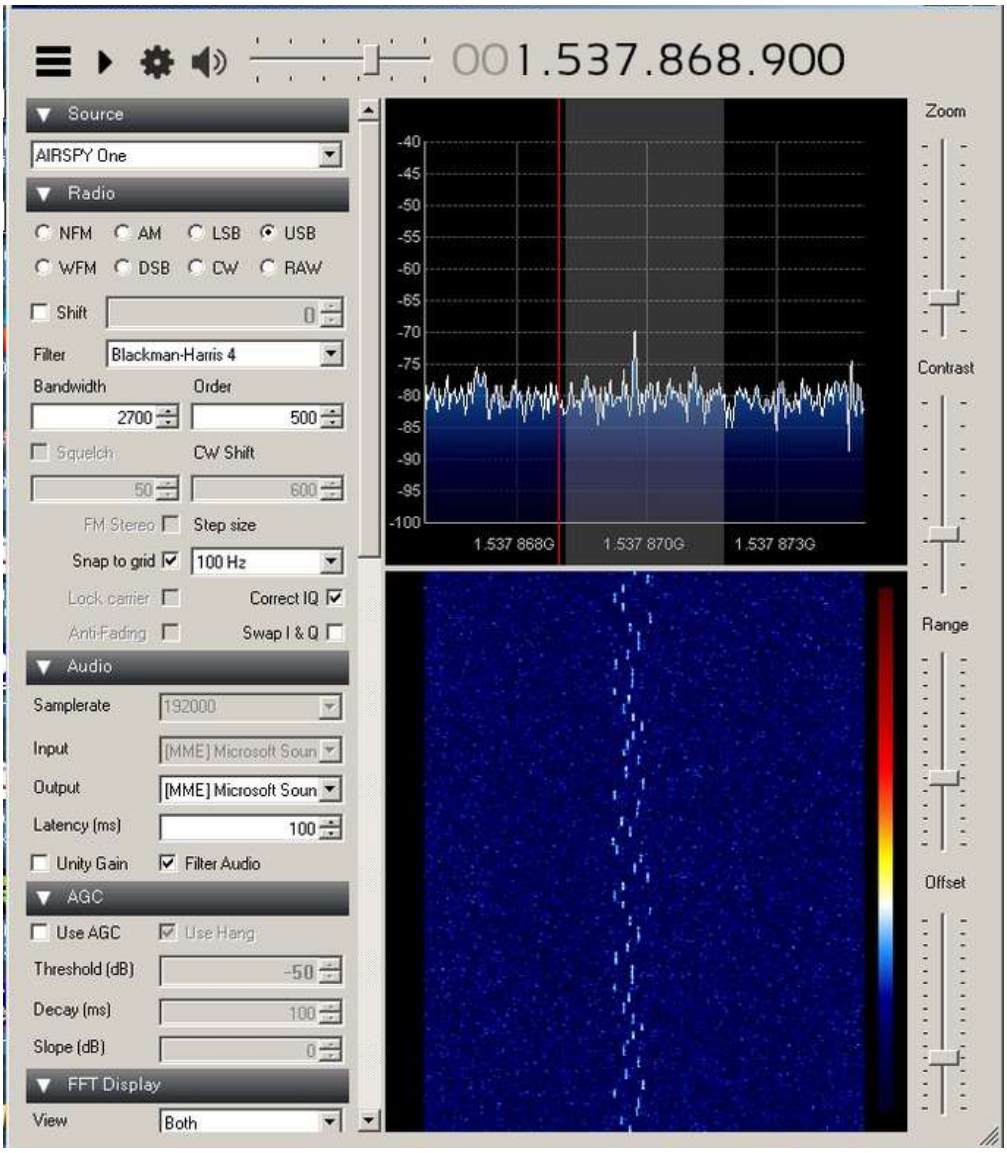

The Airspy SDR under test

February 2016

BAA, Burlington House,
Picadilly,
London
(+44)207 734 4145

Reg Charity 210769

BAA RAG Coordinator **Paul Hyde** g4csd@yahoo.co.uk
Ragazine Editor **Jeff Lashley** jeffl@spacecentre.co.uk
VLF reports **John Cook** jacook@jacook.plus.com
Web : http://www.britastro.org/radio

Notes for content submission

Content should be emailed to the RAGazine editor a minimum of fourteen days before the next publication date. Content submitted after that may not appear the next issue, but will be held for a later issue.

Observational reports are very welcome on topics where radio techniques are applied to observe astronomical objects, or geophysical events. Articles are welcome on topics of radio astronomy observational techniques, radio hardware and related technology, scientific programming, events, data processing, educational out-reach, book reviews, radio astronomy history etc.

The preferred format for submissions is Microsoft Word (.doc or .docx format). However, I know that not everyone has access to Microsoft Office, note that the free office suite LibreOffice is available for Windows, Linux and Mac OS. Note that LibreOffice can save documents in Microsoft Word .docx format. If neither of these applications are available, then plain text (.txt) is fine.

Images can be supplied embedded in the document or as separate files. Please include the author credits you require to be included in the article, and indicate whether you want your email address to be shown in the publication.

The BAA is not responsible for the opinions expressed by RAGazine contributors, and such published material does not necessarily express the views of BAA Council or RAG officers. Material without attribution is generally contributed by the editor.

Attributed material may not be copied without the express copyright permission of the author. © British Astronomical Assoc. 2014. All rights reserved

2016 Publication dates and submission deadlines

Release Date	Submission deadline
9th May 2016	25th April 2016
8th August 2016	25th July 2016
14th November 2016	31st October 2016

RAG Coordinator report

By Paul Hyde

I'm pleased to say that October's Meteor Scatter Workshop in Northampton was a great success, yet another event that sold out well ahead of the day. There is obviously a lot of interest in the subject, which I put down to a combination of accessibility (low-cost, low complexity and some resistance to local noise) and the dynamic nature of meteor activity. The day identified eight areas where amateurs can carry out serious monitoring work, whilst additional opportunities arise through combining radio observations with optical ones, in particular from the growing network of video cameras around Europe. There is now a realistic chance of tying a radio event to a specific, three-dimensional meteor trajectory, so identifying the originating meteor stream, and hence getting some idea of the structure of the meteorite, whether it is from a comet or asteroid. The radio observations can provide detailed information on the way the plasma trail dissipates, so there may be a chance of connecting this to whether the meteor is of a hard, stony construction or something more friable.

That accessibility and dynamic behaviour also makes meteor scatter attractive to a younger audience. Chris Jackson and Victoria Penrice have been working with pupils at Ratcliffe College, building meteor scatter systems and making observations. Dr Grant Mackintosh of the Tolcarn Observatory is now doing the same with Branell School in Cornwall and I provided a 45-minute talk to them via Skype. The pupils will be combining meteor scatter observing with attempts to harvest micrometeorites from rain water

Thanks to the efforts of Ian Williams we have now have a separate meteor scatter discussion group, in collaboration with the two main UK video networks, NEMETODE and UKMON, at www.radio-space.co.uk/forum/. The separate forum allows us to avoid boring the pants off those not taken with the subject. A full set of the Northampton Workshop presentations is available for download under the Useful Links so visit the site if you want to see what the fuss is about.

There's plenty else going on other than meteor scatter. In this edition you will see that Peter East continues to be active at the forefront of amateur radio astronomy, whilst the main RAG discussion group has had several mails on small dish pulsar work, though 'small' is a relative term here! We have had 12 new joiners to the Yahoo Discussion Group since the last edition of RAGazine and the current membership stands at over 250, though we hear very little of what is going on out there! There are exceptions, such as the Neutron Star Group at http://neutronstar.joataman.net, and it would be good to see details of more club/society/specialist groups so that others know what's going on.

Finally I'm aware of radio astronomy talks scheduled for Basingstoke AS (Feb 25), Gloucester ARC (Apr 11), Knowle AS (June 6) and Norwich ARC (Sept 14). Again, if you are aware of others, please let us know via the BAA RAG Yahoo Discussion Group at https://groups.**yahoo**.com/group/**baa-rag**

Best wishes

Paul Hyde

Solar Activity 3rd Quarter 2015

By John Cook

Editor's Note: Since there was no November 2015 issue of Ragazine, I include both of John's reports together, with some slight editing to avoid unnecessary duplication.

The three months in this report cover a period in which the day length (and therefore our SID observing time) becomes noticeably shorter. Despite this, July recorded the lowest SID count with 45% of the month's activity occurring on just one day. Fig 1 shows my own recording from the 6th, with the GOES X-ray flux added for clarity. A single solar active region was responsible for all of the flares shown. The final three flares are of interest as they appear to be superimposed on a much slower rise in the X-ray background level that lasted from 15:00UT to 22:00UT. This has masked the SIDs from the C2.2 and C3.5 flares, leaving just a small SID for the C4.9 flare visible at both frequencies.

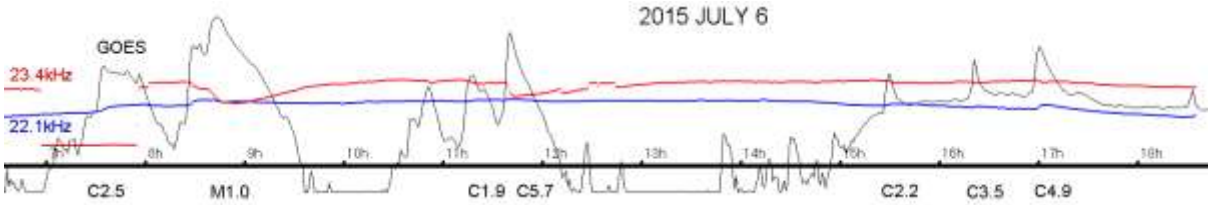

Fig 1:

The only significant CME in July was from a filament eruption at 10:40UT on the 19th. This resulted in a magnetic disturbance from 03UT to 09UT on the 23rd, with CHHSS effects adding to the disturbance later in the afternoon.

August was much more active, especially in the last two weeks as active region AR12403 rotated into view. This group was responsible for 81% of the month's SIDs. The most energetic flare of the month was an M5.6 at about 07:35 on the 24th, shown in Fig 2 along with the rest of the day's activity as recorded by Colin Clements. The red trace is 22.1kHz, blue is 23.4kHz.

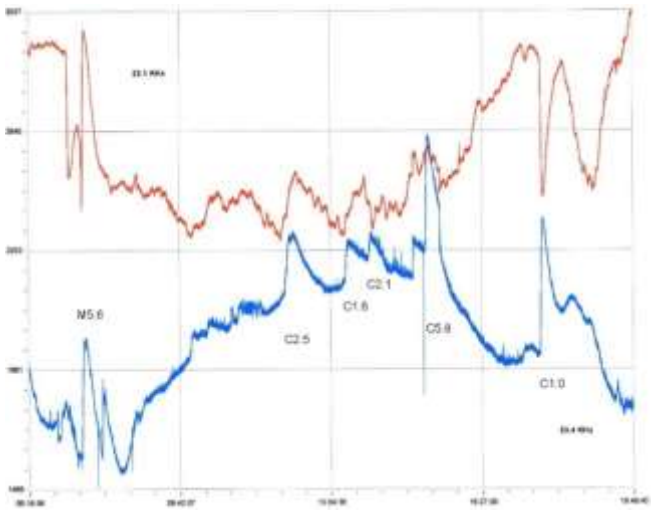

Fig 2:

An M2.2 flare peaking at 13:18 on the 28th also produced a good SID, shown in my own recording in Fig 3. A single 'shark-fin' SID is seen at 22.1kHz (blue) and an inverted 'spike and wave' SID at 23.4kHz (red).

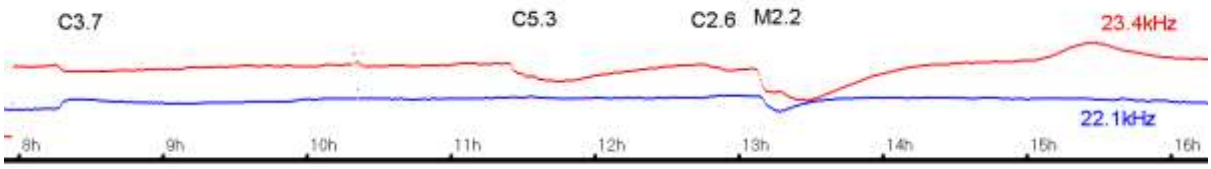

Fig 3:

Magnetic activity in August was also mostly in the last two weeks, with an extended period over the 26th to 28th, illustrated in Fig 4 by Roger Blackwell. A large coronal hole was present over all three days, producing an increase in solar wind speed. The M1.2 flare on the 22nd added to this with an Earth-directed CME. Although the CME was fairly weak, added to the already present CHHSS it produced quite a large disturbance. Coronal holes are becoming the major source of magnetic disturbance as the current solar cycle wanes. Sudden polarity changes in the solar wind can link directly with the Earth's magnetic field, creating sudden changes in the ionospheric current and conductivity. They can also produce some subtle SID-like features at VLF as shown in Fig 5. The upper trace is from Mark Edwards (Coventry) and the lower trace is from G4JVF in Chesterfield. A C9.5 flare is marked, but the feature at 19:40 marked '*' is not related to any flare, but does coincide with a magnetic polarity change.

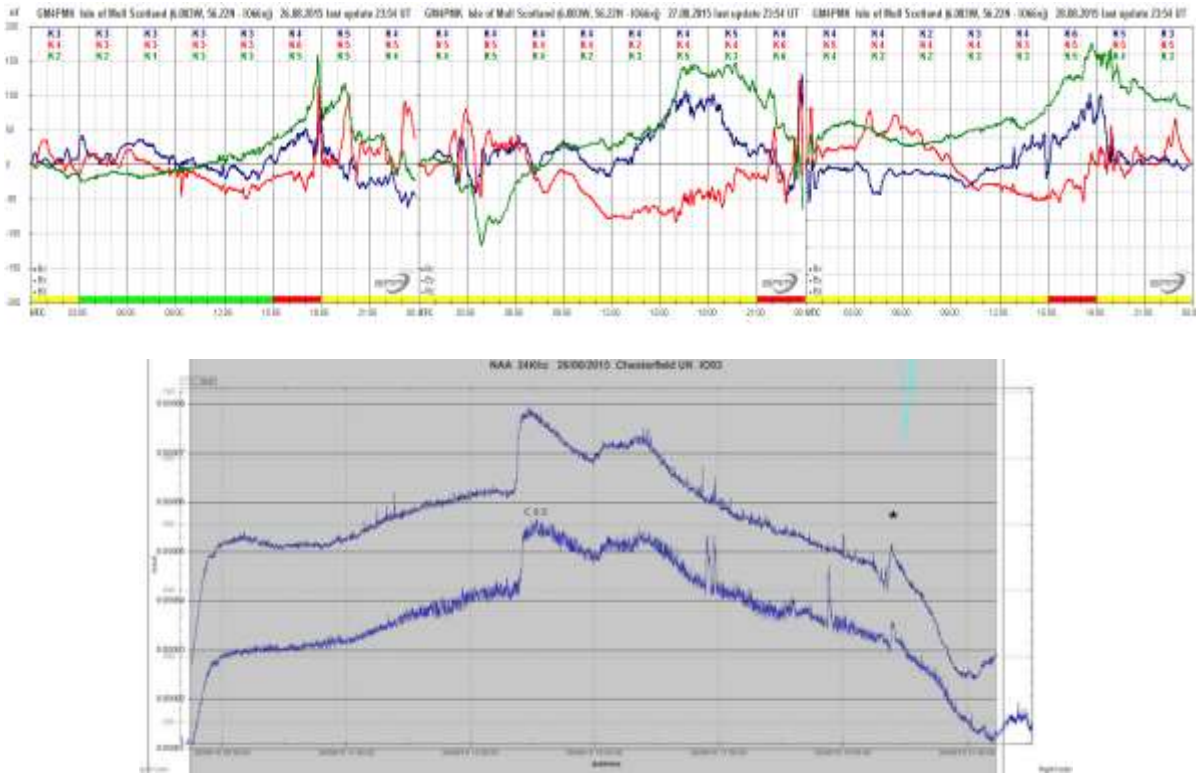

Fig 4 (top) & 5

A similar event was recorded by Mark Edwards on September 11th, shown in Fig 6. Data from the 12th has been overlaid as a reference. A strong response can be seen peaking at 09UT on the 11th, followed by a series of waves. Both 19.6kHz and 22.1kHz show the effect, with opposite polarities. On this occasion a large equatorial coronal hole producing a fast flowing solar wind was responsible. Data from the Hartland magnetic observatory of the British Geological Survey shows a sudden change in magnetic declination along with a strong dip in horizontal intensity at 09UT. X-ray flux was at a very low background level over this period, allowing the solar wind to dominate.

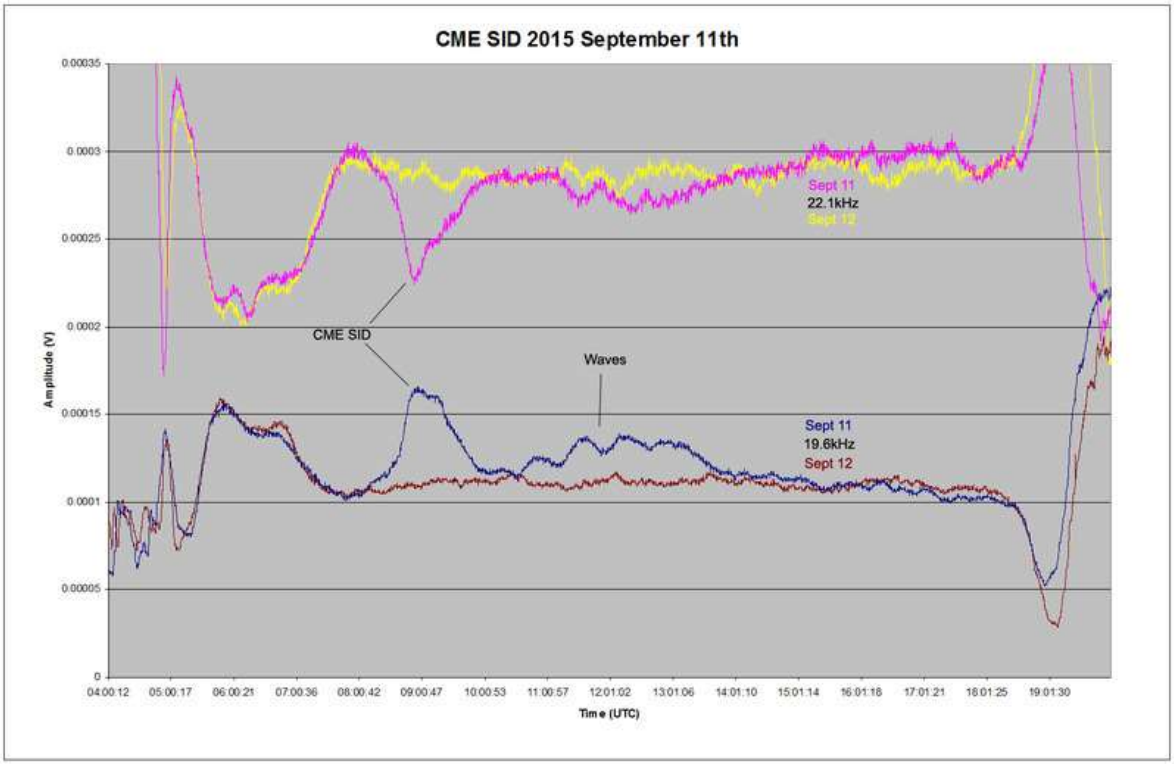

Fig 6:

Although the SID count for September was down on August, they were mostly compressed into the last ten days of the month. A strong M7.6 flare was recorded at about 15:00UT on the 28th, illustrated in Fig 7 by Paul Hyde. The SID from the M7.6 flare has a very sharp rise compared to the earlier M1.1 flare. This was much slower with three peaks, the middle one being the M1.1.

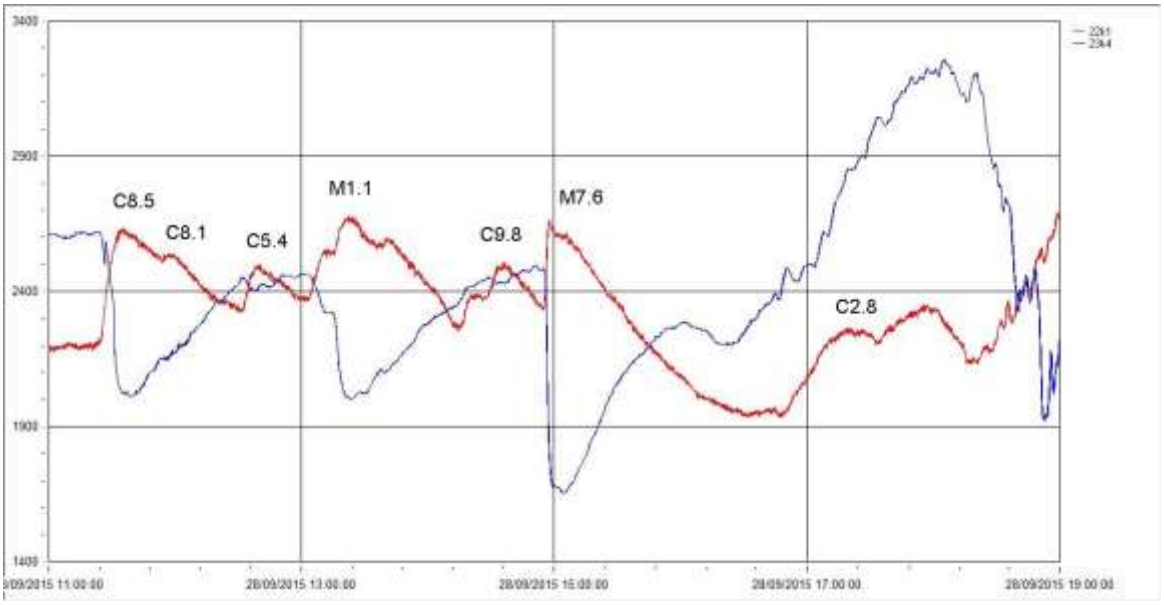

Fig 7:

Magnetic activity in September was again mostly from Coronal hole effects. A combination of a filament eruption and a CHHSS led to some very disturbed conditions over September 7th to 9th. Starting mid-afternoon on the 7th, the magnetosphere was very active until about 03UT on the 8th. After a quieter period through the afternoon of the 8th, it again became quite active into the 9th. All was quiet again by the afternoon of the 9th. Despite several very strong flares during September there were no large CME impacts recorded; those flares that did produce CMEs were mostly aimed away from Earth.

Solar Activity 4th Quarter 2015

Fig 8 shows activity levels since 2005. Sunspot numbers are courtesy of the BAA Solar Section. SID numbers since the last report are as follows: -

- July 21 (including 3 M-class).
- August 65 (including 9 M-class).
- September 49 (including 11 M-class).
- October 62 (including 5 M-class).
- November 13 (including 3 M-class).
- December 9 (including 2 M-class).

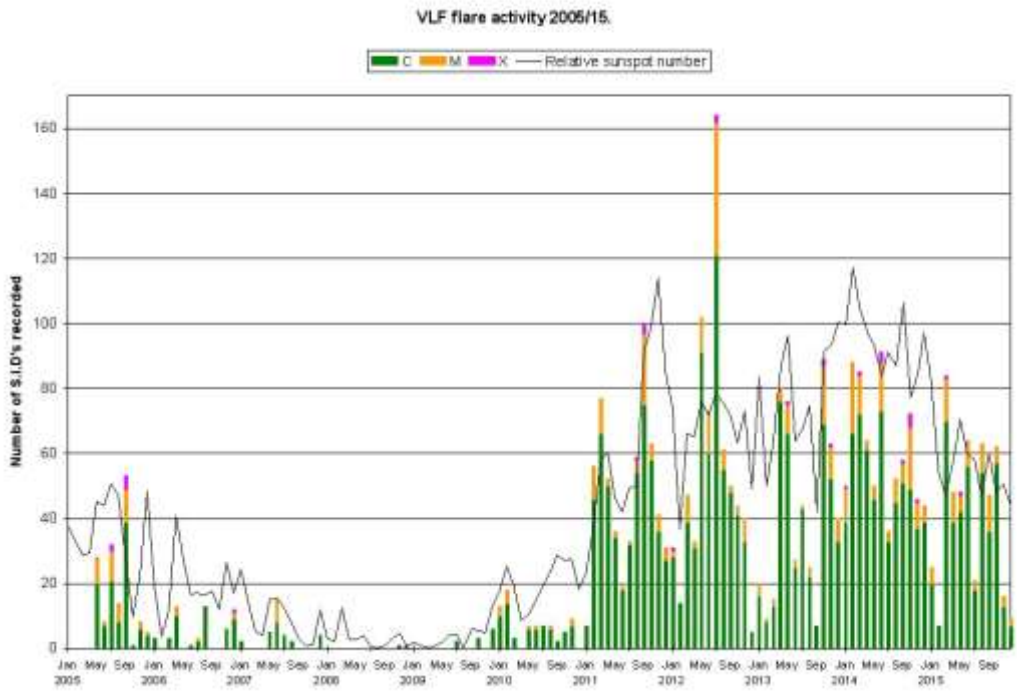

Fig 8:

October was by far the busiest month covered in this report. A strong M4.5 flare was recorded on the 1st, along with two smaller events, shown in Fig 9 by Colin Clements. The SID from the early C3.5 flare is inverted compared to that from the M4.5 flare, while the C7.7 flare has produced a more complex SID where the sky-wave path length has changed by greater than 180 degrees. Strong activity continued on the 2nd, with ten flares recorded. Fig 10 is Colin's recording showing some of the day's activity, again with a mix of inverted and more complex SIDs. Six much weaker flares were recorded on the 3rd, followed by a ten day gap with nothing recorded. Activity then slowly increased again, with eight flares being recorded on the 30th.

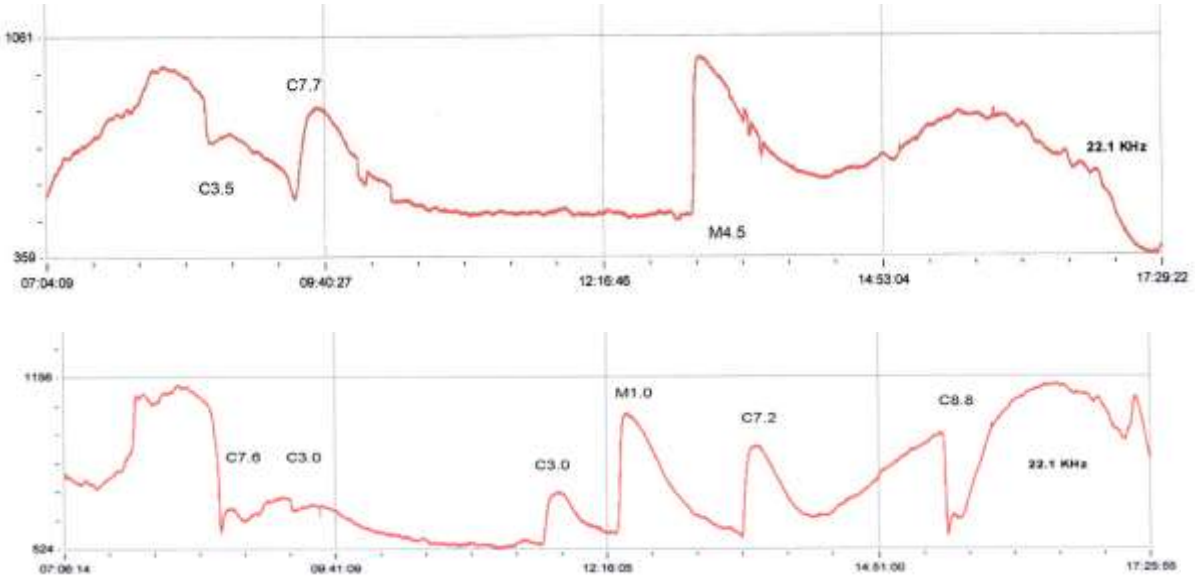

Fig 9 (top) & 10

Mark Edwards noted a pair of SID-like features at 24kHz on October 7th that were clearly not related to flare activity. Fig 11 shows his recording, with data from the 6th overlaid in white for comparison. The first peak at 16:50UT on the 7th matches with a strong increase in Solar wind speed from 400km/s to nearly 800km/s as measured by the ACE satellite. The magnetic shock from the increased speed has caused the ionospheric electron density to increase, and so producing a SID. The long (>4500km) path at 24kHz is ideal for seeing these features, as the ground wave is so much weaker, leaving the sky wave to react to ionospheric conditions. High speed winds from coronal holes were present through most of October, with just a single CME reported on the 22nd.

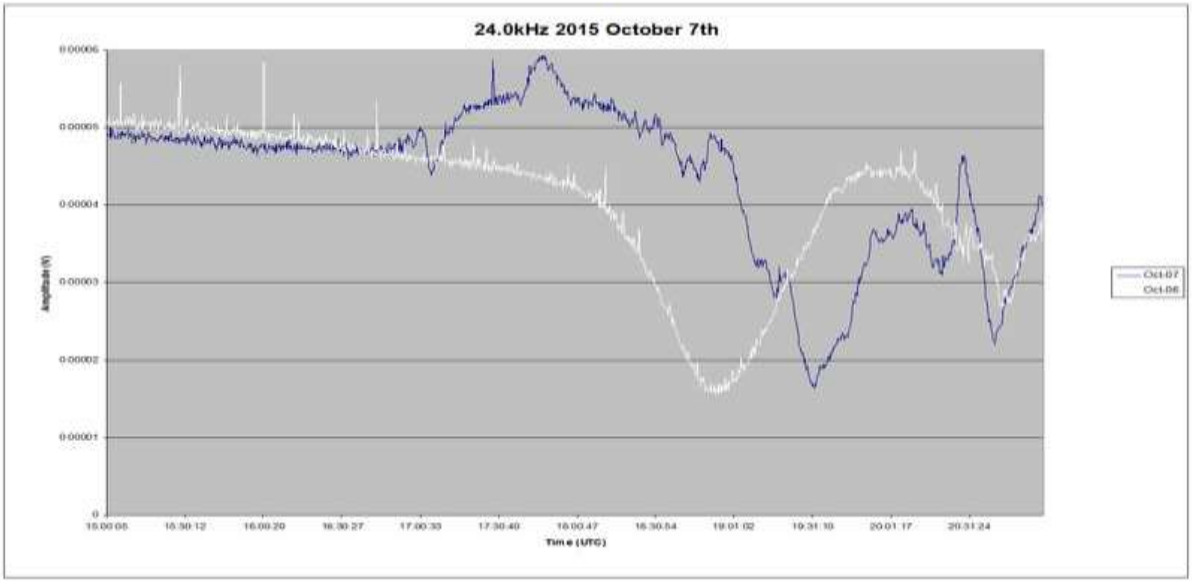

Fig 11:

Activity in November was restricted to just the first ten days of the month. Fig 12 shows November 4th, recorded by Mark Edwards. This is a very complex chart at first glance with seven signals recorded, and just three SIDs. Perhaps the cleanest of the signals is that at 20.27kHz (purple trace) from Isola di Tavolara, Italy. This path is about 1500km, and again has a weaker ground wave compared to the more local signals. Each of the three SIDs is clearly defined although small in amplitude. 24kHz (dark blue) shows the two M-class flares, but looses the earlier C4.6 flare in the sunrise disturbance. The other signals are quite strongly disturbed by general noise, often seen at this time of year on the shorter paths as the solar altitude reduces through winter.

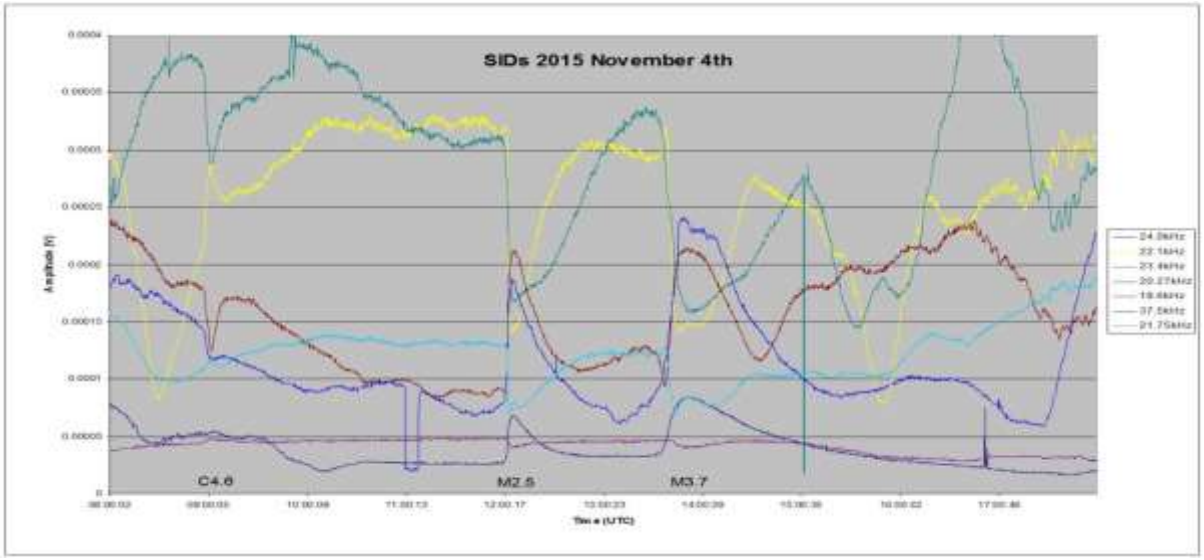

Fig 12:

The M2.5 flare on November 4th was accompanied by an Earth-directed CME that arrived on the 6th. My own recording showed a SSC at 18:19UT, with a disturbance of about 10nT. This was followed by a much stronger magnetic disturbance on the 7th, shown in Roger Blackwell's magnetogram, Fig 13. Our timings give a CME transit time of 54 hours 5 minutes. This CME came against a background of coronal hole activity through the first half of the month. A second CME resulted from a pair of filament eruptions that combined to give a disturbance on the 18th and 19th.

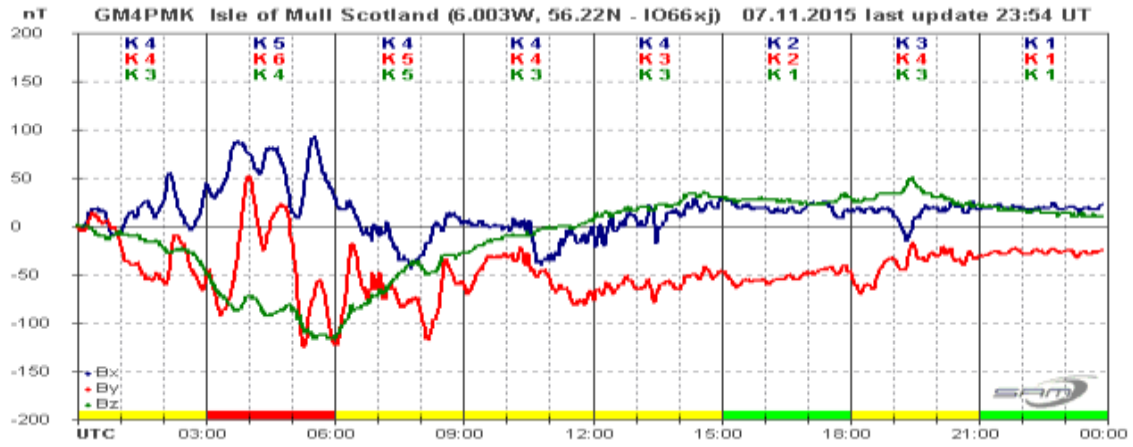

Fig 13:

December was much quieter, with 9 SIDs recorded. A major feature has been the winter noise and oscillations against a background of generally low solar activity. Fig 14 is Colin Clement's recording from the 21st, showing a very high noise level, all but obscuring the M1.1 flare at 10:10UT. The background X-ray flux was about B7/B8 during the day, with the sun at its lowest altitude of the year in the northern hemisphere. Mark Edwards also noted periods of more sustained oscillation with a period of about 5 minutes, again often seen with the sun low in the sky.

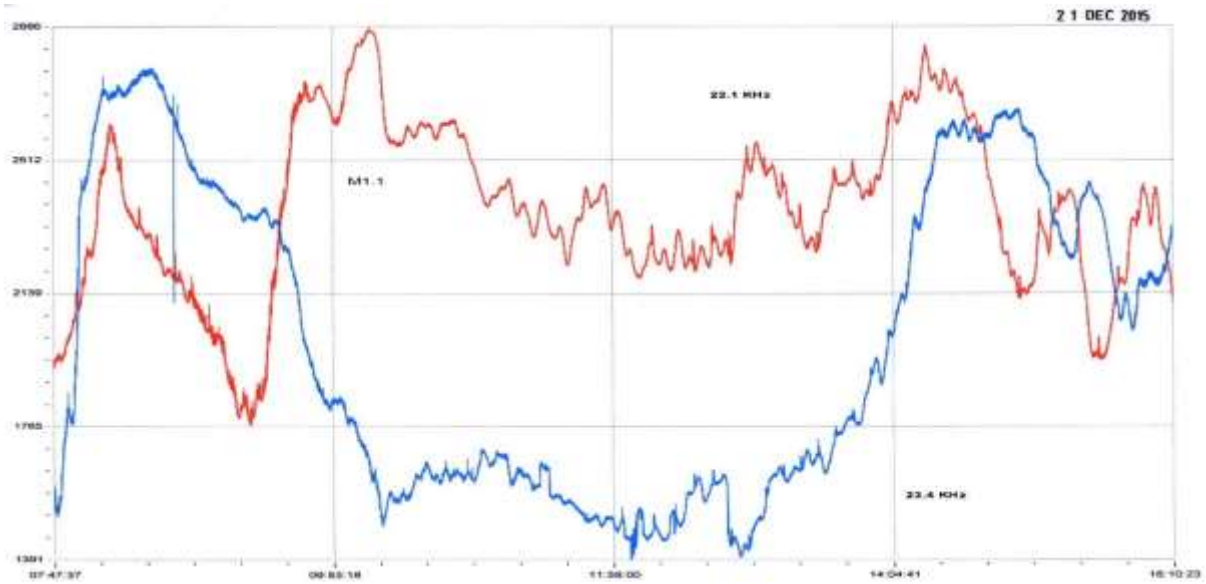

Fig 14:

We did record much more magnetic activity however, mostly from CHHSS effects. The most active period resulted from a pair of CMEs on the 16th. A C6.6 flare at 09:24 (not recorded as a SID) produced the first CME, followed by a filament eruption at 14:36 that produced the second CME. A very well defined SSC was recorded by Roger Blackwell at 16:16 on December 19th, followed by a major disturbance on the 20th as shown in Fig 15. Note the change in vertical scale between the two days in this chart. The disturbance lasted until about 09UT on the 21st. An M1.8 flare widely recorded as a SID

at 12:26 on the 28th also produced a CME. We recorded an SSC 60 hours 24 minutes later at 00:50 on the 31st, followed by a magnetic disturbance lasting into the New Year. Both events produced some good aurora, A picture of New Year fireworks in Scotland against a background aurora appeared on the spaceweather web site.

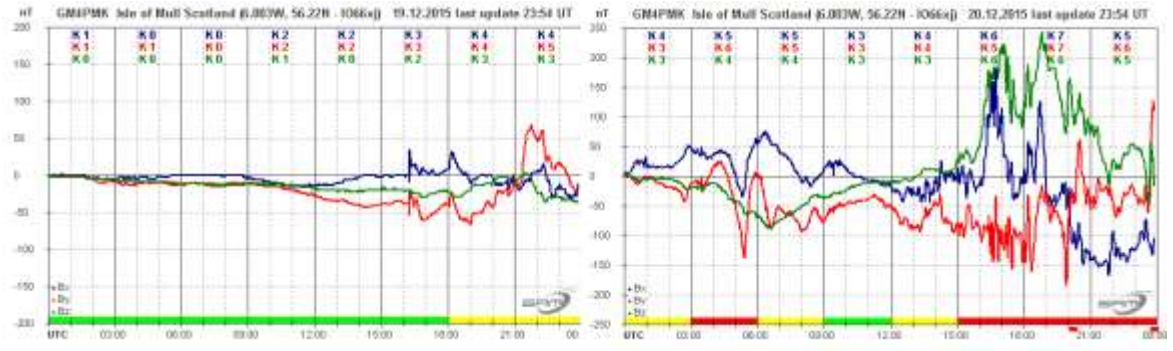

Fig 15:

As usual, Mark Edwards has produced a chart of D-region height through the year from his modelling software, Fig 16. The overall shape is very similar to that in previous years, although the raw data does show a lot more variability compared with previous years. The model is based on measurements at 19.6 and 22.1kHz, raw data being in red and the model output in green.

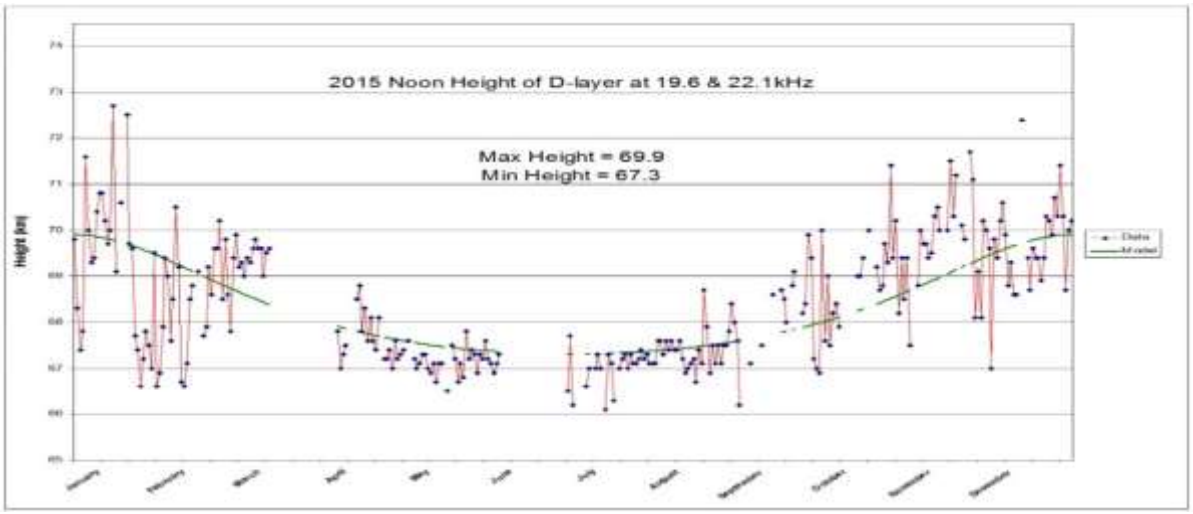

Fig 16:

A full description of these events as well as listings of SID timings can be found in my monthly VLF summaries, copies of which can be seen on the Radio Group website.

Observers: Roberto Battaiola, Jim Barber, Roger Blackwell, Colin Clements, Mark Edwards, John Elliot, Paul Hyde, Steve Parkinson, Phil Rourke, Gonzalo Vargas, John Wardle and John Cook. My thanks to all contributors. If you would like to add your own observations, please contact jacook@jacook.plus.com.

February **2016**

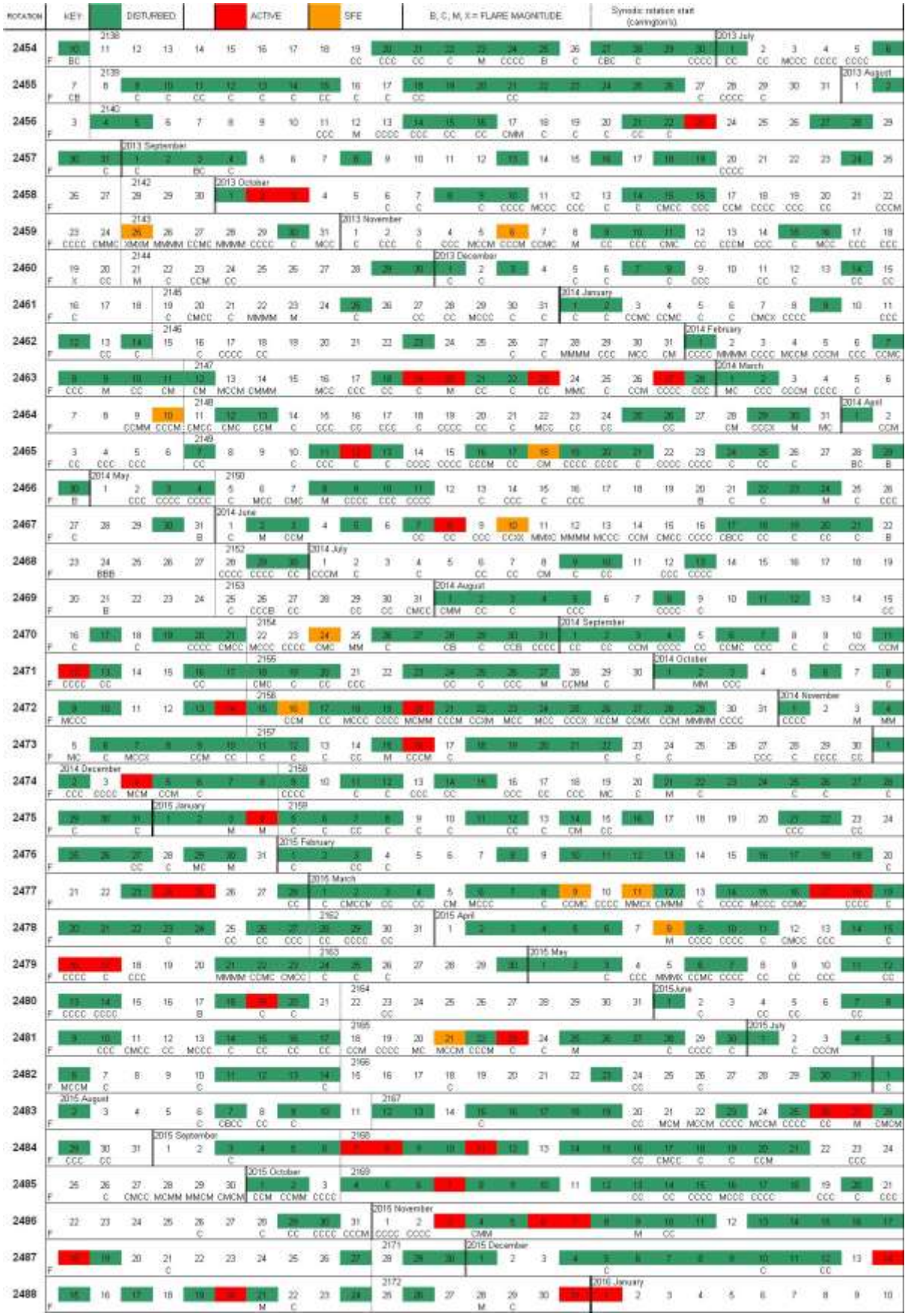

February 2016

Estimating Radio Telescope Antenna Sidelobe Temperature

By Peter East

Abstract

Practical radio telescope antennas generally intercept ground radiation in their side/back-lobes especially when tilted towards the horizon or towards trees/buildings. Given the 3D antenna beam pattern it is possible to integrate over offending regions to determine ground effects on the system noise temperature[1]. This note describes a simpler technique for antennas with circular symmetry using measured or estimated co- and cross-polar patterns.

Definitions

1. *Antenna Noise Temperature*

From Reference 1, the antenna noise temperature equation for an antenna placed in a non-zero temperature environment that accounts for antenna cross polarisation is,

$$T_A = \frac{\int_0^{2\pi}\int_0^{\pi}\left[P_C(\theta,\phi)T_{bC}(\theta,\phi)+P_X(\theta,\phi)T_{bX}(\theta,\phi)\right]\sin\theta d\theta d\phi}{\int_0^{2\pi}\int_0^{\pi}\left[P_C(\theta,\phi)+P_X(\theta,\phi)\right]\sin\theta d\theta d\phi} \quad (1)$$

where, $P_C(\theta,\phi)$ and $P_X(\theta,\phi)$ are power per unit solid angle for co-polar and cross-polar antenna response respectively and $T_{bC}(\theta,\phi)$ and $T_{bX}(\theta,\phi)$ are the surrounding brightness temperatures.

This is equation is implemented in a simpler quantised form below to allow a good working estimate of the ground temperature contribution to the telescope system temperature.

$$T_{SA} = \frac{\sum_{g=1}^{G}\left(T_{Cg}G_{Cg}SA_{Cg}+T_{Xg}G_{Xg}SA_{Xg}\right)}{\sum_{g=1}^{G}\left(G_{Cg}SA_{Cg}+G_{Xg}SA_{Xg}\right)} \quad (2)$$

G_{Cg} and G_{Xg} represent relative main and sidelobe gain levels, assumed constant over solid angles, SA_{Cg} and SA_{Xg} (steradians)

[1] http://bookzz.org/s/?q=Noise+Temperature+Theory+and&t=0

2. *Antenna Directivity (Gain)*

Given a spherical set of antenna polar pattern measurements, the antenna directivity can be calculated from,

$$D = \frac{4\pi\left[P_C(0,0) + P_X(0,0)\right]}{\int_0^{2\pi}\int_0^{\pi}\left[P_C(\theta,\phi) + P_X(\theta,\phi)\right]\sin\theta\, d\theta\, d\phi} \qquad (3)$$

As before, this equation can be simplified using the quantised integration technique to,

$$D = \frac{4\pi\left(G_{C0} + G_{X0}\right)}{\sum_{g=1}^{G}\left(G_{Cg}SA_{Cg} + G_{Xg}SA_{Xg}\right)} \qquad (4)$$

This directivity figure includes pattern focusing efficiency and will exceed the measured gain by resistive and mismatch losses.

Antenna Sidelobe Number Concept

Ignoring resistive losses and loss due to illumination profile, the maximum gain of an aperture antenna, area *A*, is given by the well-known formula,

$$G = \frac{4\pi A}{\lambda^2} \qquad (5)$$

where λ is the signal wavelength.

For a square aperture side *D*, $A = D^2$.

Now λ/D is the antenna beamwidth = BW in radians. So we can re-write the Gain equation as,

$$G = \frac{4\pi}{\left(\frac{\lambda}{D}\right)^2} = \frac{4\pi}{BW^2}$$

Now observe that there are 4π steradians in a sphere and BW^2 is approximately the antenna main beam solid angle, also in steradians.

Similarly, for a circular reflector, G becomes,

$$G = \frac{4\pi}{\left(\frac{\lambda}{D}\right)^2} = \frac{4\pi}{\left(\frac{\pi BW^2}{4}\right)} \approx \frac{4\pi}{BW^2}$$

So the gain equation is also telling us that the antenna can be considered as producing a number of radial beams, numerically equal to G over the 4π sphere. One of course is the main directional beam and the G-1 remainder can be thought of as much lower level side and back-lobes equi-spaced over the surface of the sphere; each lobe emanating from the centre of the sphere.

This is a useful concept as it means that we don't have to do any 3D integration over the side-lobes to determine power radiated or temperature sensed in sidelobes.

We can set a level to the G-1 sidelobe beams from measurements or antenna knowledge and just sum the sidelobe/equivalent beam contributions over their relevant solid angles.

Calculating Sidelobe Temperature Contributions

If the antenna pattern is assumed rotationally symmetric, a particular sidelobe region can be thought of as a number of equivalent sidelobe beams occupying an open spherical sector of a sphere as shown in Figure 1.

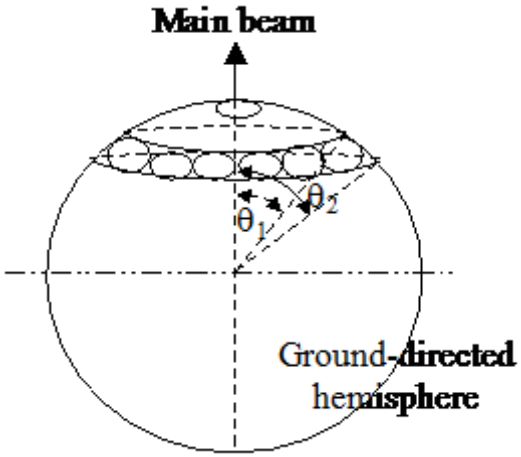

Figure 1 Sidelobe solid angle (SA) θ_2 - θ_1 spherical sector definition

The solid angles covered by a particular sidelobe level region are calculated from the open spherical sector, solid angle formula,

$$SA = 4\pi\left[\left(\sin\frac{\theta_2}{2}\right)^2 - \left(\sin\frac{\theta_1}{2}\right)^2\right] = 2\pi(\cos\theta_1 - \cos\theta_2) \quad (6)$$

where, θ_1 and θ_2 represent the specified sidelobe sector (elevation) limits.

From this solid angle we can calculate the equivalent number of sidelobe gain beams within it,

No. of sidelobe beams, = $$N_{sl} = \frac{SA.G}{4\pi} \quad (7)$$

Adapting Equation (2), and assuming the antenna is singly polarised and placed in a closed environment with the walls at 290°K, the temperature resulting from a particular equivalent sidelobe beam is,

$$T_{sl} = \frac{290.G_{sl}.N_{sl}}{\sum_{g=1}^{G} G_g N_g} \quad (8)$$

where, G_{sl} is a nominated sidelobe beam boresight-relative gain, N_{sl} is the number of equivalent sidelobe beams at this level and the denominator represents the sum of the power levels of all *GN* lobes.

The method is demonstrated with an example. In this case, based on an 8deg beamwidth reflector antenna with published gain 23dB (~x200). The maximum possible gain using the specified beamwidth = 29dB ~ x822.

The overall efficiency then, is 25%, (-6dB gain from maximum = 1/4). Efficiency losses of a focus fed parabolic dish include feed losses, illumination profile loss. Directivity losses include spillover and power lost in sidelobes.

Example

The example co-polar antenna pattern of a parabolic reflector antenna is shown in Figure 2. For the following calculations, it is assumed that this pattern is preserved in the boresight axis of revolution.

The pattern is first divided into a number of angular regions by eye, where the sidelobe levels appear roughly constant, (Column 1, Table 1). Column 2 represents the mean sidelobe level over each region. Column 3 is the calculated solid angle (Equation 6) whilst Column 4 lists the equivalent number of beams (Equation 7), in this case totalling 822, the calculated maximum gain.

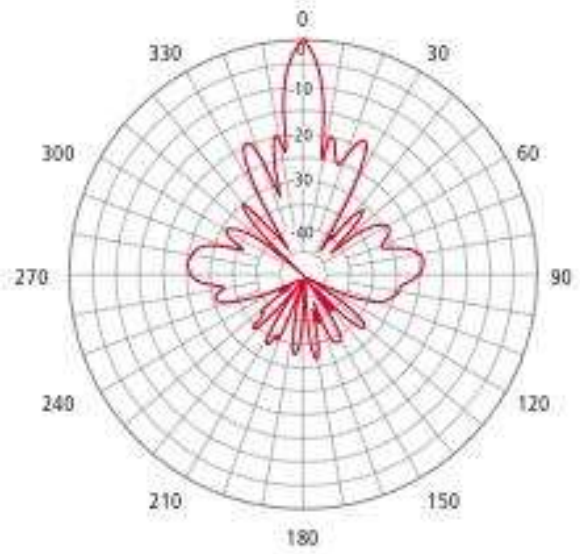

Figure 2 Polar Pattern of Parabolic Dish Example

Angle (deg)	SL Level (dB)	Solid Angle (Steradians)	No. Beams	Lobe Temp
0-4	0	0.015	1	132
4 -10	-15	0.1	5	21
10-30	-25	0.75	49	20
30-75	-30	3.8	250	33
75-95	-25	2.2	142	59
95-110	-30	1.6	105	14
110-180	-35	4.1	270	11
Totals		-	**822**	**290**

Table 1 Calculation of sidelobe temperature contributions

The lobe temperature contributions, Column 5 are calculated using Equation (8), where $\sum_{g=1}^{G} G_g N_g$ = 2.207, the sum of all the lobe power level beam number products.

The table shows that 55% of the power enters through the sidelobes and the antenna pattern efficiency is 45% (=132/290) and accounts for 3.4dB gain loss from the ideal.

The other 2.6dB (ideal gain 29dB, published gain 23dB in the example is reflector illumination loss, feed antenna efficiency etc:

This example shows that with the rear hemisphere facing the ground, side/backlobes can contribute 25° or more to a radio telescope system temperature. The region 75° - 95° should be kept well clear of ground/building/tree obstructions.

Estimating System Ground Temperature with Tilted Antennas

When tilting the antenna away from the vertical, the proportion of relevant angle ranges directed at ground/warm structures can be estimated and sidelobe sections summed to obtain a new sidelobe temperature result. Pointing an antenna horizontally towards the horizon for example, half the antenna pattern hemisphere is now ground-directed, which would result in a ground temperature contribution of 290/2 = 145°K.

BW-Az	BW-El	Max. Gain	Min Angle	Max Angle	Mean level (dB)	Xpol level	SA (sterads)	No: of Beams	CPxT	XPxT	C Power	X Power	C Temp:°K	C+X Temp:°K
28.8	28.8	18.01	0	10	0	-30	0.095	0.48	139.499	0.139	0.481	0.000	81.985	75.25
			10	20	-3	-27	0.284	1.43	207.620	0.827	0.716	0.003	122.02	112.33
		63.3	20	30	-10	-26	0.463	2.33	67.642	1.699	0.233	0.006	39.75	37.37
			30	40	-17	-26	0.628	3.17	18.317	2.306	0.063	0.008	10.77	11.11
			40	50	-21	-27	0.775	3.90	8.990	2.258	0.031	0.008	5.28	6.06
			50	60	-24	-26	0.897	4.52	5.219	3.293	0.018	0.011	3.07	4.59
			60	70	-22	-28	0.993	5.00	9.152	2.299	0.032	0.008	5.38	6.17
			70	80	-27	-25	1.058	5.33	3.084	4.889	0.011	0.017	1.81	4.30
			80	90	-30	-27	1.091	5.50	1.594	3.181	0.005	0.011	0.94	2.57
			90	100	-25	-25	1.091	5.50	5.041	5.041	0.017	0.017	2.96	5.43
			100	110	-23	-27	1.058	5.33	7.747	3.084	0.027	0.011	4.55	5.84
			110	120	-22.0	-25	0.993	5.00	9.150	4.586	0.032	0.016	5.38	7.40
			120	130	-25.0	-27	0.897	4.52	4.145	2.615	0.014	0.009	2.44	3.64
			130	140	-30.0	-25	0.774	3.90	1.131	3.577	0.004	0.012	0.66	2.54
			140	150	-32.0	-27	0.628	3.16	0.579	1.831	0.002	0.006	0.34	1.30
			150	160	-27.0	-25	0.463	2.33	1.348	2.137	0.005	0.007	0.79	1.88
			160	170	-23.0	-27	0.283	1.43	2.073	0.825	0.007	0.003	1.22	1.56
			170	180	-21.0	-30	0.095	0.48	1.103	0.139	0.004	0.000	0.65	0.67
Totals							12.6	63.3	493.436	44.727	1.702	0.154	290.00	290.00

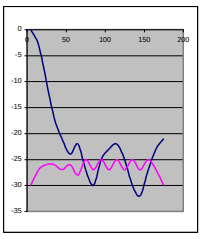

Notes:
1. Adjust black bold font entries only
2. Max linear gain = 52525/Az/El
3. Number of beams in 4pi steradians = linear gain
4. Side/backlobe temp: from rear hemisphere (90-180) in Tsys = 30.26 deg K
5. Antenna pattern efficiency = 77.6 %

Figure 3 Sidelobe Spreadsheet Table - Yagi Array Example

A convenient and simple approach is to divide the Table 1 angle range into a number of equal divisions and to input the data into a spreadsheet[2] as shown in Figure 3. This example uses data calculated for a 22-element Yagi antenna and includes the antenna cross-polar response.

The method of estimating the system temperature due to ground illumination of the antenna sidelobes is to assume that ground temperature source always occupies the lower hemisphere as seen by the antenna pattern. With this stipulation, when the pointing direction of the antenna is tilted from the vertical new halves of the sidelobe sectors fall within this region whilst on the opposite side, the other half-sectors enter the forward hemisphere. Using this simple algorithm, and summing the lower hemisphere sectors, an estimate of how the ground influences the system temperature with tilting is realised. Figure 4 shows the tilting ground system temperature using the data of

Tilt °K	Tilted Temp:	Incl: Cross Pol:
0	**18.99**	**30.26**
10	**17.98**	**28.83**
20	**16.61**	**28.06**
30	**16.61**	**27.44**
40	**16.93**	**27.92**
50	**19.24**	**29.68**
60	**24.45**	**34.59**
70	**43.93**	**52.33**
80	**104.33**	**107.71**
90	**145.00**	**145.00**

Figure 4 System Ground Temperature Variation with Antenna Tilt from Vertical

Figure 4. Column 2 and 3 list ground-directed hemisphere noise temperature; column 2, co-polar response only, column 3 including a simulated cross-polar response.

As an example of calculating the values in Figure 4, the result for a 10° tilt using just co-polar data from Figure 3 ('C Temp' column) is,

17.98 = SUM(C Temp 100° to 180°) + ½.SUM(C Temp: 80° to 100°)

Refer to the .xls file in footnote [(2)] for more detail.

Figure 4 shows that antenna cross-polar performance can have a significant effect on the ground-induced system noise temperature. Although the cross-polar figures for this antenna were estimated, it does show that they need to be much lower than the co-polar sidelobes to minimise their effect. It is interesting to note that the ground system temperature does not change significantly for tilts up to 50°

Conclusions

The note describes a simple approximate method of estimating the effect of side/back-lobes and cross-polar performance on degrading the system temperature of a radio telescope over most practical tilting angles. The concept of considering an antenna as generating G lobes and weighting and summing these over areas of interest is a useful aid although sidelobe weighted integration of the open spherical sectors is just as valid.

Reference

[1] Lambert, K. M., and R. C. Rudduk, "Calculation and Verification of Antenna Temperature for Earth-Based Reflector Antennas," *Radio Science*, Vol. 27, No. 1, January–February 1992, pp. 23–30.

[2] http://www.y1pwe.co.uk/RAProgs/SidelobeTempYG4C.xls

RFI Interference and Pulsar Detection

By Peter W East

Introduction

This note follows on from the paper Amateur Pulsar Detection[1] and investigates the effects of RF interference on pulsar detection SNR. Whilst the synchronous integration/folding technique (*rapulsar.exe*) is an excellent period tuning discriminator for noise and interference suppression when recovering the pulsar pulse, RF interference (RFI), if close in frequency to the pulsar period can seriously impair the period matching process, especially for weak pulsar signals.

An investigation into RFI mitigation using a 1 GB Vela pulsar data file supplied by GM Gancio[2] has shown that a useful improvement in SNR is obtained by narrow-band harmonic filtering the RFI before applying the folding algorithm. Considering the example in Figure 1 but now using 98 bins, the SNR change was from 61 with no filtering to 69 with some RFI filtering. However, the process did offer albeit a small improvement in pulsar pulse visibility, and so is described.

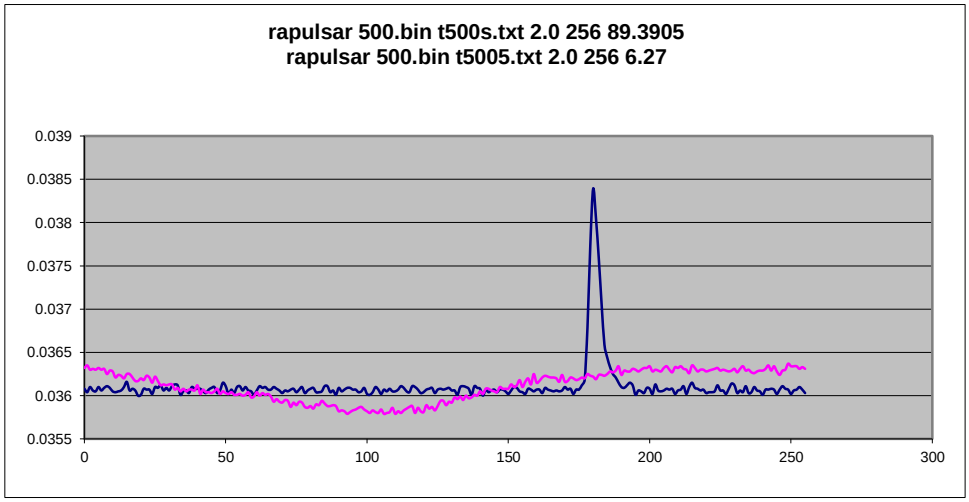

Figure 1 Vela folded pulse (blue) and main interference component (magenta)

Also plotted in Figure 1 is one cycle of the main RFI component (magenta; interference period 6.27ms) - this was recovered by using the folding technique, primed now with the interference period rather than the pulsar period. In this case, the pulsar signal is suppressed as are other RFI components.

[1] Amateur Pulsar Detection. PW East & GM Gancio. BAA RAGazine Vol 3, Issue 1, Aug. 2015.
http://www.britastro.org/radio/ragazine/RAGazine_2015_Aug.pdf
http://www.y1pwe.co.uk/RAProgs/AmateurPulsarDetectionF.doc

[2] Institute of Radio Astronomy, Argentina.

Examining RFI

RFI spectral components were identified by applying and FFT to the data after first downsampling it from 2MHz to 1kHz, using *pdetect* software[1] using the command line,

pdetect *500.bin pdet500.txt 2.0 1.0 1*

The first 131072 samples in this data file were then spectrum analysed in a 131072-point Real FFT in MathCad and the result is plotted in Figure 2.

In this strong signal data, the pulsar spectral lines and RFI components are clearly seen. The pulsar line harmonics, at FFT bin_n are related to the pulsar period and FFT properties from,

$$bin_n = \frac{Qn}{TB_v}$$

where, Q = number of FFT points, T = the pulsar period and B_v the downsizing video bandwidth (1kHz)

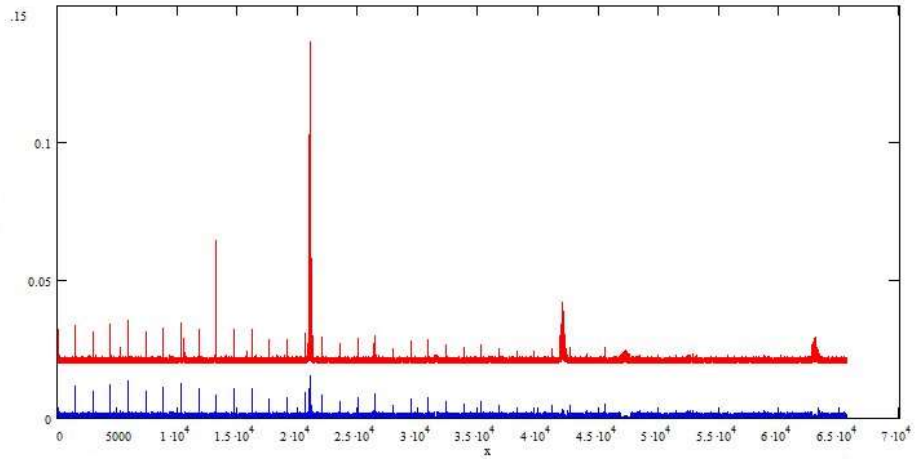

Figure 2 Data File 500.bin Real Spectrum (red).

Blue Plot:- manually reduced RFI by 20dB

In this example (Figure 2), bin numbers expected to contain pulsar modulation harmonics, are 0, and Int[*n*.1466.286], where *n* = 1,2,3 ….etc:, and Int[] represents the integer part. Bins containing the larger RFI components are easily identified and attenuated or removed by manually adjusting a set of digital bin-blocking filters.

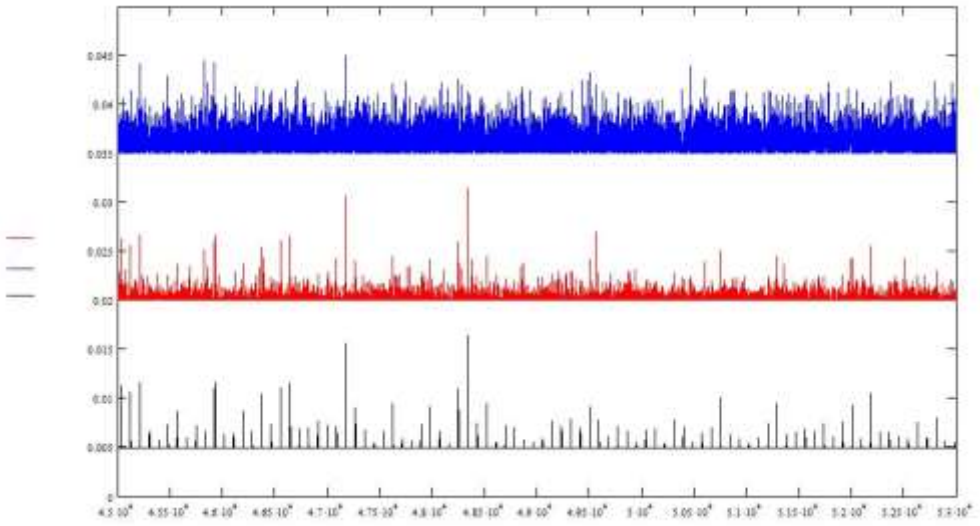

Figure 3 Data Plots, blue: raw data; red: RFI filtered data; black: pulsar pulses

From Figure 3, it is clear in the RFI filtered data (red) that the larger pulsar pulses are much more visible and there is some pulsar amplitude scintillation evident. The red filtered time plot was obtained by taking the inverse FFT of the filtered spectrum data.

In the third (black) plot many more lower level pulsar pulses can be identified and the process to obtain this will now be explained.

Extracting Individual Pulsar Pulses

By setting up a narrow-band harmonic repeating filter gate about the pulsar spectral lines and then taking the inverse FFT of this data, the pulsar pulse train modulation at the pulsar period can be extracted and plotted as shown in the red plot of Figure 4.

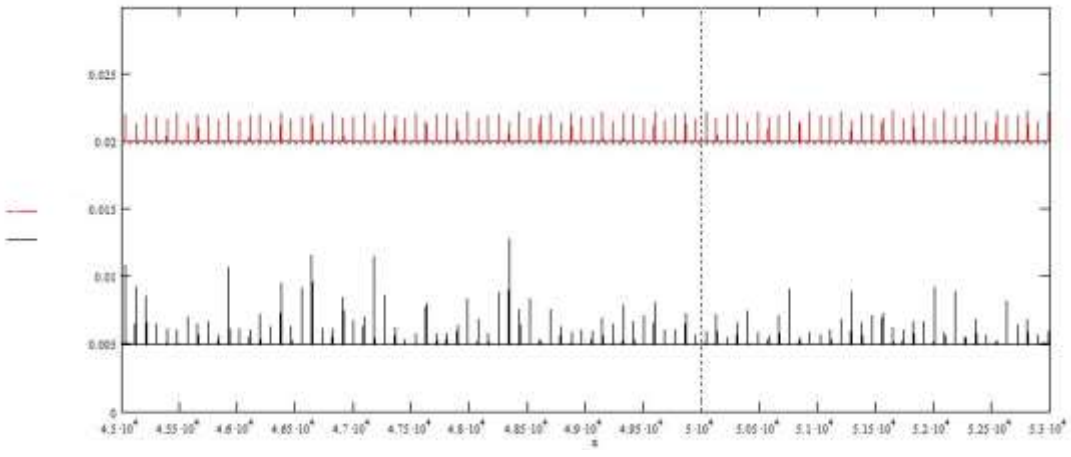

Figure 4 Data Plots, red: pulsar modulation; black: pulsar pulses

In fact, this data exhibits the pulsar pulse modulation shape and phase but without the individual pulse amplitudes. The amplitude data, however can be recovered by using this pulse train to control a harmonic time gate, selecting the pulsar pulses from the filtered time data giving rise to the black plot of pulsar pulses; now including amplitude and pulse shape. Detail is shown in Figure 5. Note small individual pulses can still be corrupted system residual RFI and noise.

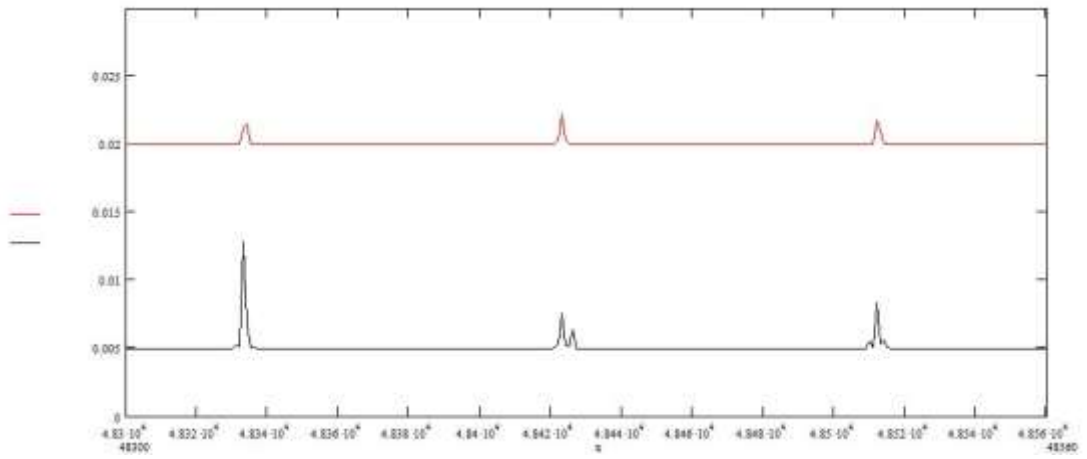

Figure 5 Pulsar Pulse Modulation Detail

Conclusions

This document has described the processes required to identify and remove the main RFI components from the data spectrum.

On strong signals and where the RFI harmonics do not clash with the pulsar spectral components, a useful improvement in SNR is possible. However, with weak signals, although pulsar period and spectral components may be known, RFI filtering may not always be effective.

Extracting pulsar modulation properties by filtering, inverse transforming and then time gating gives useful information on amplitude scintillation of strong pulsars. The filtered data can then be folded to produce and improved SNR.

A Test of Airspy at 1537MHz compared with FCDpro and plus

By Tony Abbey

The Airspy USB receiver has recently come on to the market. It is a similar price ($199) to the FunCube Dongle receiver, but is capable of displaying a full 10MHz B/W from 24 - 1800 MHz. It uses the 820T tuner chip, but unlike Howard's FCD it doesn't have a low noise preamp.

An attractive feature for RA work is that the 10MHz reference oscillator can be provided externally, and also the internal ARM code is public domain so new applications can be provided, such as generating spectra internally in the receiver, rather than externally in the PC.

This test was undertaken to see how its noise around the hydrogen line frequency compared with the excellent performance of the FCDpro+.

SDR# can process many different types of SDR input, including the Airspy and FCD, using an amplified GPS patch antenna, which can receive Inmarsat telemetry directly. The patch antenna was placed on an external windowsill at the side of the house facing the geostationary Inmarsat satellite. The internal bias-t of Airspy and FCDpro+ allow power to be fed to the antenna.

The tests

I could receive some multi-frequency telemetry signals using both FCDpro and plus, the plus version gave 12dB S/N ratio, and pro 10dB; well done Howard! Also they both showed around 5dB noise increase from the powered antenna at 1537.8MHz. However, the Airspy was much noisier, using 2.5 Mbps and decimation x 64' to make it as quiet as possible, could only see around 0.5dB extra noise from the antenna, and could barely see the telemetry signals. I did find one signal about 10dB above noise, but the same signal on the FCD was 15dB above noise. After playing with the gain controls, it was no better even at max.

My FCDPro+ has Howard's 1/2 speed firmware (for my Raspberry Pi) which is sampling at 96000 sps, it was then I realised the S/N ratio gets even better with the sample rate in SDR# set to 96000 as well, instead of the default of 192000 I then got 17.5dB S/N.

The effective sample rate on the Airspy was 39.062 Ksps. If I change to decimation of 32 to give a rate of 78.125 Ksps then the S/N drops to 7.5dB, a full 10dB worse than the FCD. The FFT factors remained the same, Blackman-Harris 4 resolution 4096.

I guess with the usual low noise amps for H-line astronomy, this will be OK, but so far, I am a little disappointed.

The first image below shows the FunCube Dongle Pro+ at 96000 sps giving 17.5dB S/N ratio, and the second the Airspy at 19200 sps with 7.5dB S/N.

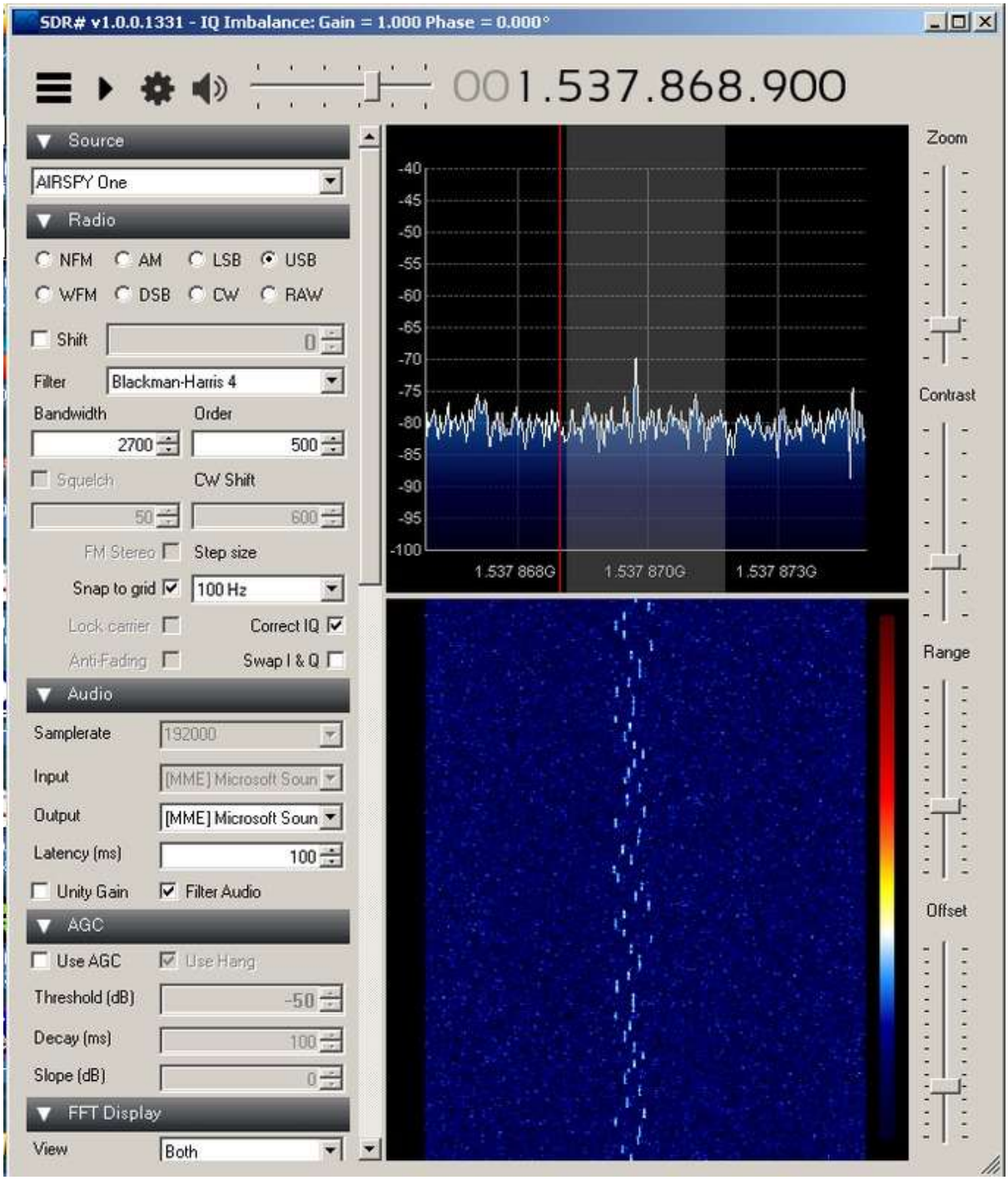

AirSpy_Inmarsat.jpg

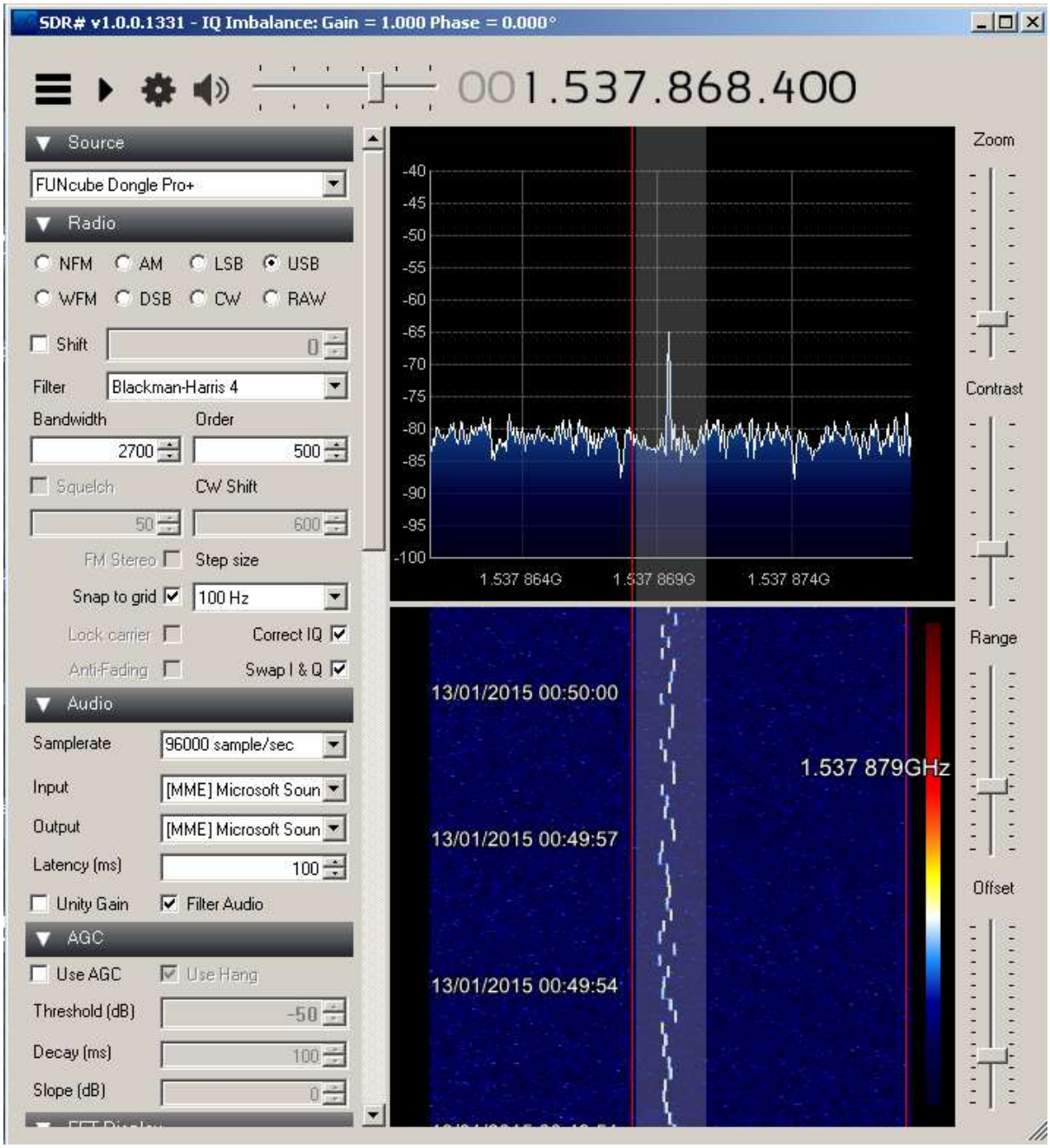

FCDpro+_Inmarsat_2.jpg

There is another aspect of the Airspy which might cause a few problems. The designer (Youssef) says that it should not be used with older slower PCs and Windows XP. In fact, it can, but the audio stutters if the interface is run at 10Msps, but is OK at 2.5Msps. To utilise the full bandwidth which the Airspy provides, a modern high spec PC is needed. This might be a problem for wideband radio astronomy applications, but probably not with narrow band H-line reception.

Reducing the effect of interference when detecting meteor scatter events

By Paul Hyde

The August edition of RAGazine carried an article describing how the use of Spectrum Lab's *new_spectrum* flag can be used to overcome the problem of random data being saved for short duration head echoes. Another common problem is various forms of interference creating false triggers, thus distorting the meteor activity profile. This piece describes further developments to reduce these false triggers and to support the use of the Scatterthon application for reviewing the event log and removing any remaining errors.

How Spectrum Lab detects meteors

Spectrum Lab and similar applications use an algorithm called a Fast Fourier Transform to convert a series of measurements (samples) of the amplitude of a signal into a representation of its frequency spectrum. In mathematical speak, the FFT transforms from the time domain (the series of samples) to the frequency domain. The output from the FFT is a series of values showing how much energy is contained in different frequency 'bins', each bin having a frequency range of a few Hertz wide.

The usual practice for detecting meteor events is to look at a narrow range of frequencies (the Trigger Band) around where the meteor pings fall and identify the frequency bin containing the highest value. This value is then compared with a background noise level derived from the values of all the frequency bins across the Trigger Band. If the maximum signal exceeds the noise level by a pre-set margin (I use 17 dB) then the system registers an event start and starts to take measurements.

This method works well in rejecting false triggers from impulse noise spikes such as those generated from a light switch or fridge thermostat. The signal level registers the increase from the spike, but the reference noise level also goes up and so prevents a trigger being registered. However, narrow band interference signals from monitors, broadband modems and a hundred other domestic items will generate a trigger if they are strong enough and fall within the Trigger Band limits.

Reducing the Trigger Band width

Assuming that you cannot identify and remove the cause of the interference, the easiest way of reducing false triggers is to narrow down the frequency band that you look at, so that it excludes any problem signals – see Fig 1. This cannot protect you against interfering signals at frequencies close to those of the meteor pings, but it can significantly improve the situation for those further away or that drift through the waterfall.

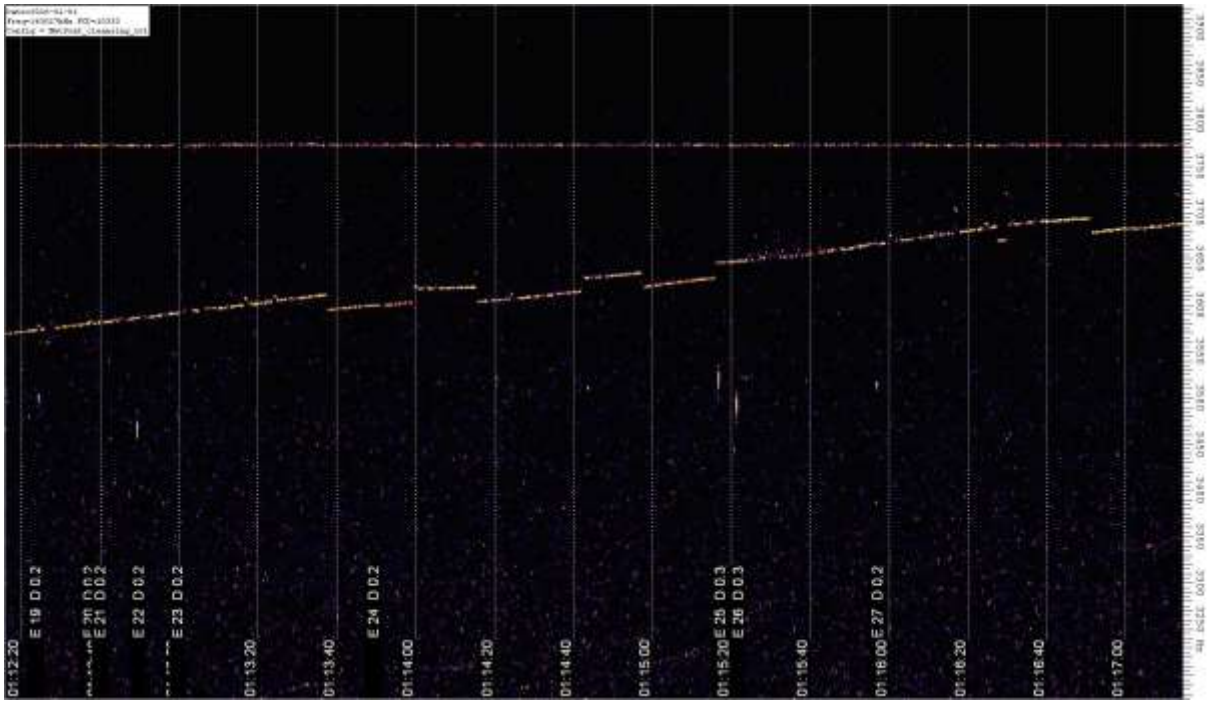

Fig 1 Reducing the Trigger Band reduces the number of false detections from interfering signals

I initially tried narrowing the trigger band to just 50 Hz above and below the frequency of the illuminating transmitter (the Centre Frequency). This worked well for the large majority of meteor events, but experience with the 2015 Geminids showed a few head echoes with large Doppler shifts were being missed so I increased it to plus or minus 100 Hz.

This value could be narrowed further when observing meteors using the BRAMS (49.97 MHz) or VVS (49.99 MHz) meteor beacons since the lower frequencies result in lower Doppler shifts. I haven't done any work here but I would think that plus or minus 40 Hz would be an appropriate starting point.

Improving the noise reference mechanism

A problem with narrowing the trigger frequency range is that a large event or a powerful head echo can completely fill it, thus looking like a broadband noise pulse and causing the trigger mechanism to ignore it – see Fig 2. Richard Fleet uses a completely separate range of frequencies to obtain a noise reference figure and this approach is adopted here. This Noise Band needs to be close enough to the trigger band to track the background noise level, but far enough away to avoid being saturated by a big Doppler shift event.

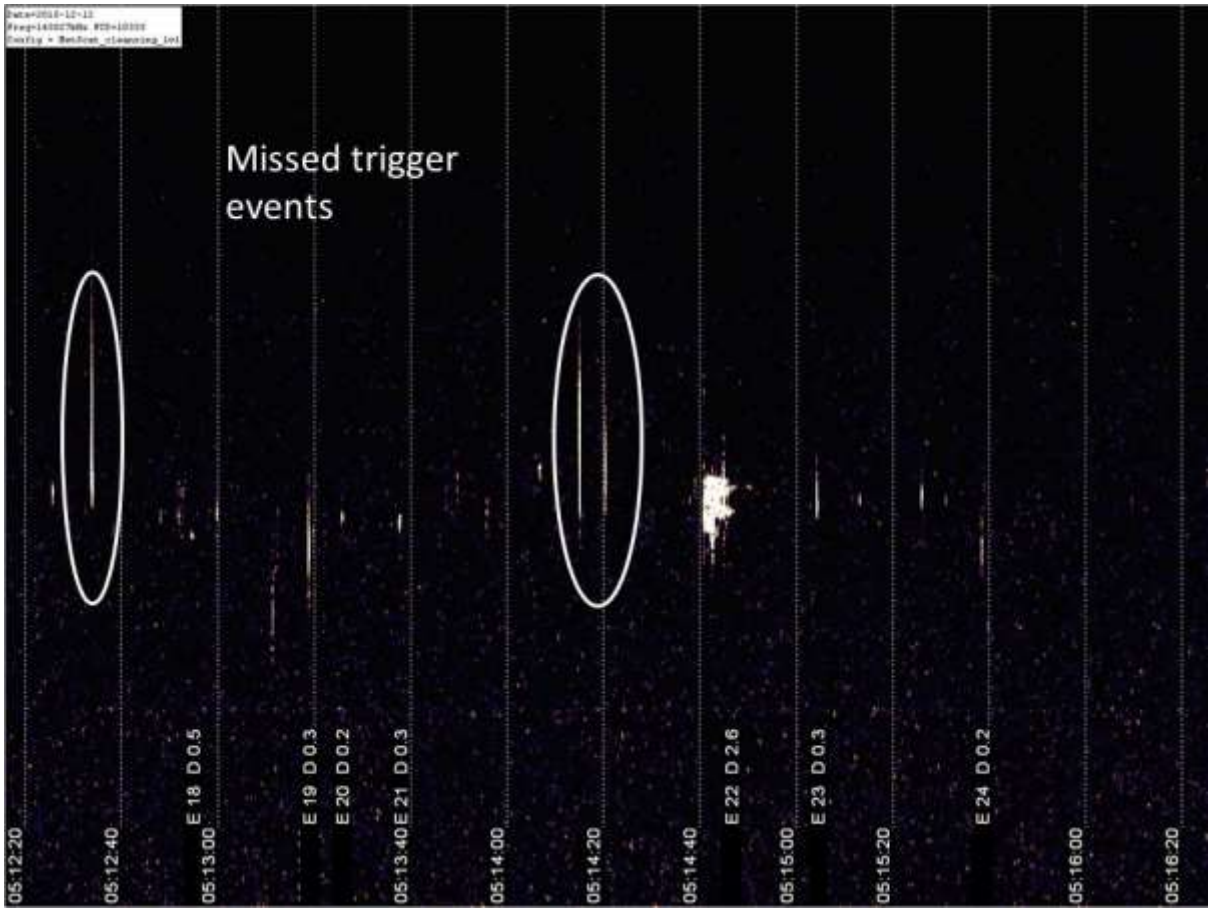

Fig 2 Deriving a reference noise level from a narrow Trigger Band runs the risk of a head echo filling the band and looking like a broadband noise spike, thus supressing a trigger

I use a 100 Hz wide Noise Band lying between 200 Hz and 100 Hz below the reference frequency. Most (but not all) meteor head echoes descend in frequency, so looking below the band occupied by meteor pings is a safer approach. However, if you suffer from an interfering signal in the designated Noise Band then you could modify the values to look either lower still or even switch to a 100 Hz band above the Trigger Band.

Simplifying set up

Most observers adjust their receivers so that meteor pings are centred around 1 kHz, which is at the most comfortable part of the audible range. However, if you are not going to listen to the pings you can chose a higher frequency and this can be another way of dodging interfering signals that enter the system after the antenna. Using a Centre Frequency of 2 kHz is recommended for the FUNcube Dongle receiver as the internal noise level increases below around 500 Hz. However if you are going to change the receiver offset, you need to modify the Trigger Band limits to track the change in the frequency of the meteor pings. Using a different band for noise measurements adds another two figures to be modified, with a consequential risk of error and resulting change in the sensitivity of the system.

The Spectrum Lab Conditional Actions (CA) script can be used to calculate the limits of the Trigger and Noise bands so that the user only has to enter the Centre Frequency, i.e. the frequency at which the illuminating transmitter would appear if it was received directly, say due to Tropospheric Scatter. So for

a conventional communications receiver set for 143.049 MHz the user would enter 1000 as the Centre Frequency and the CA script would monitor a Trigger Band lying between 900 and 1100 Hz, and obtain a Noise reference from the band between 800 and 900 Hz.

If the receiver is set for 143.048 MHz the user would enter 2000 as the centre frequency, which will result in a Trigger Band of 1900 to 2100 Hz and a Noise Band of 1800 to 1900 Hz.

For the FUNcube Dongle Pro Plus receiver you will also need to take account of the frequency error that is associated with individual receivers, usually in the range of 200 to 500 Hz. Establishing this value should be part of the initial setting up of a new receiver and is best done using a known frequency reference, such as one of the amateur radio beacons. This only has to be done once as the offset stays stable to within a few Hz once the device has warmed up.

It is important that the Conditional Actions script is re-initialised every time the Centre Frequency is changed or else the new values will not be applied. This can be done using the "Init" button on the left of the Conditional Actions page. The current value of the individual parameters can be checked by 'floating' the screen cursor over the relevant parameter, whereupon its current value will appear against the 'Test Line' window at the bottom of the CA page.

Coping with receiver frequency drift

Spectrum Lab displays the frequency spectrum of the signal fed to it from the receiver. If the receiver is subject to frequency drift as it warms up, or as the ambient temperature changes over the day, then the meteor pings will also drift up and down the waterfall screen. If the drift is severe enough the pings will drift outside of the narrow Trigger Band limits suggested above and detections will be lost.

Good quality receivers such as the ICOM R7000 and FUNcubeDongle Pro Plus do not drift excessively once they have reached their normal operating temperature. This is not the case for receivers such as the PCR1000 or the budget TV dongles that are sometimes used for meteor scatter work. The problem can be controlled by limiting the change in ambient temperature around the receiver, so keeping it away from central heating radiators, out of the sun, and away from drafts. The dedicated observer could put the receiver in a temperature controlled enclosure to achieve adequate stability. Beginners should be aware of the issue and watch out for the effects, namely the way that meteor pings drift up and down the screen. Comparing screenshots is a good way of doing this. If meteor pings are found to be drifting outside of the trigger limits the options are to widen the trigger band and risk increased interference, relocate the receiver to somewhere with a more stable temperature, or upgrade!

Supporting a review process

Whilst narrowing the trigger range will reduce the number of false triggers, it cannot remove errors completely. Any interfering carrier that appears in or crosses the Trigger Band will always generate a false trigger if it is strong enough. The options then are to reposition the antenna to reduce the level of the interfering signal or to manually remove false entries from the Event Log. This requires a complete visual record of the day's activity.

It is easy enough to use Spectrum Lab to save regular screenshots to build up a daily record. This can be done using either a Conditional Actions command or by using the Periodic Actions feature – see Fig 3. The latter is simpler to set up and has the advantage that time-synchronous screenshots can be implemented across multiple computers, which helps any subsequent comparison process.

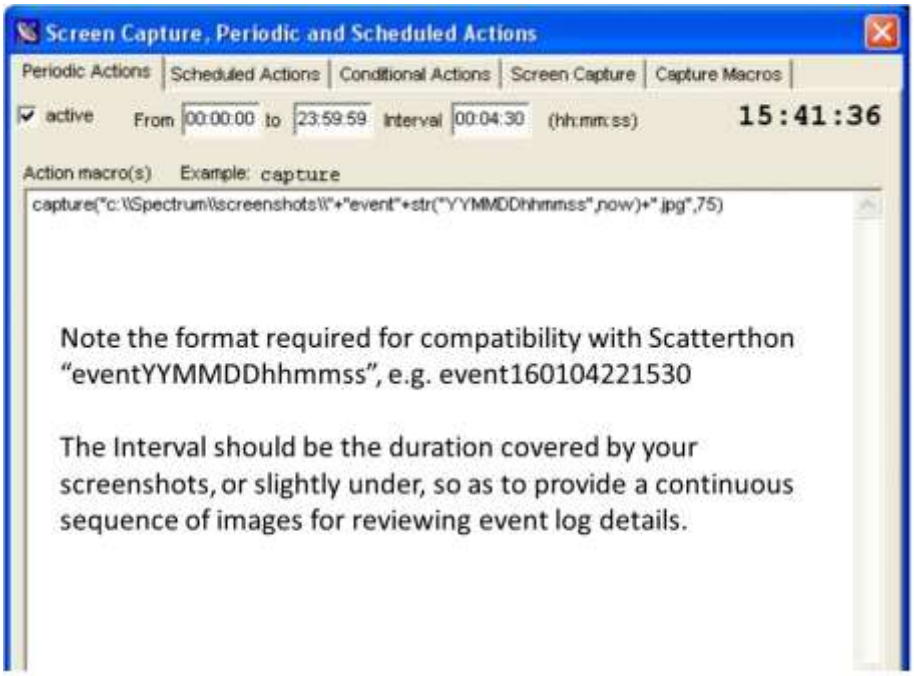

Fig 3 Using the Periodic Actions function to take a complete set of screenshots for subsequent verification of the event log details

Reviewing a day's event log now requires cycling through the screenshot images and identifying errors. This sounds daunting, but experience shows that it can be completed within 15 minutes for a normal day's activity, provided that there are not too many interfering events. Experience with the 2016 Quadrantids showed that this can stretch to nearly an hour when you have several thousand meteor events during a day. Victoria Penrice and Chris Jackson are currently developing the Scatterthon application which displays event logs alongside screenshots and keeps them synchronised as you work through the day. It also allows you to classify and remove non-meteor events from the output file and split or merge individual events if needed.

Using Spectrum Lab's VFO offset feature

By looking at meteor pings in the frequency domain we can determine the Doppler shift imparted by the moving meteor. This then tells us the Line of Sight velocity of the meteor and its resulting train, though it does not give us absolute velocities.

It is possible to enter the value of the Centre Frequency used in the Conditional Actions script into the vfo offset field at the top left hand corner of the main Spectrum Lab waterfall screen – see Fig 4. By selecting the *Include VFO offset* option Spectrum Lab will subtract this value from the displayed frequency range. A meteor reflection with zero Doppler shift will now appear on screen at 0 Hz, whilst the reflections from meteors or meteor trains moving away from the observer will appear at negative frequencies. The value of the frequency shift can also be read off using the screen cursor.

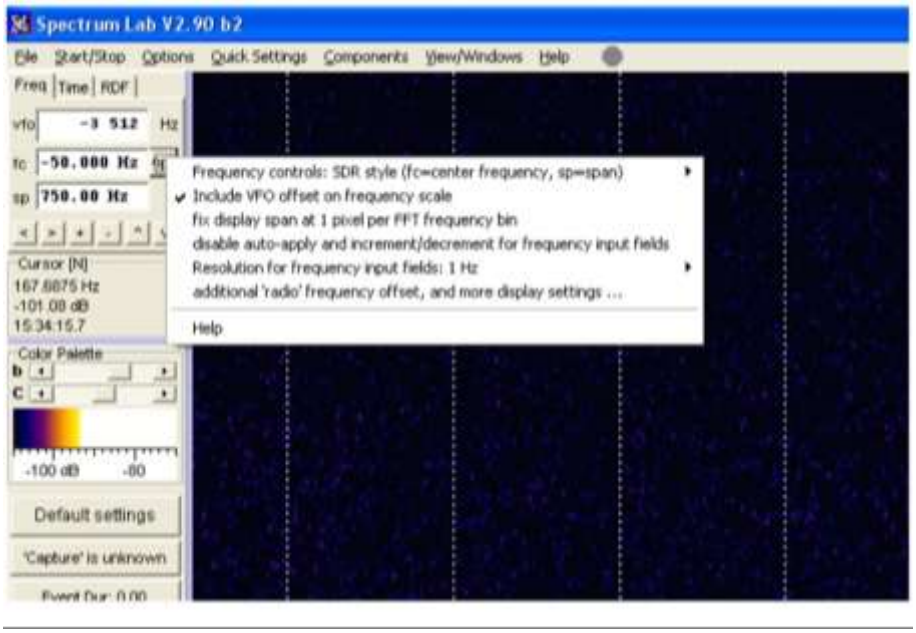

Fig 4 Enabling Spectrum Labs vfo offset feature

Some people may like using this feature, whilst others may not. The subtraction of the vfo frequency value only applies to the displayed frequency and does not affect any values saved to the event log, though it could do so if required.

The revised Conditional Actions script also subtracts the Centre Frequency from the recorded Trigger Frequency to obtain a Doppler value which is printed on the screen – see Fig 5. This proves to be very useful when checking data as it can indicate whether an event trigger is due to a true meteor event, and hence should be retained, or to a nearby interferer and hence needs reclassifying.

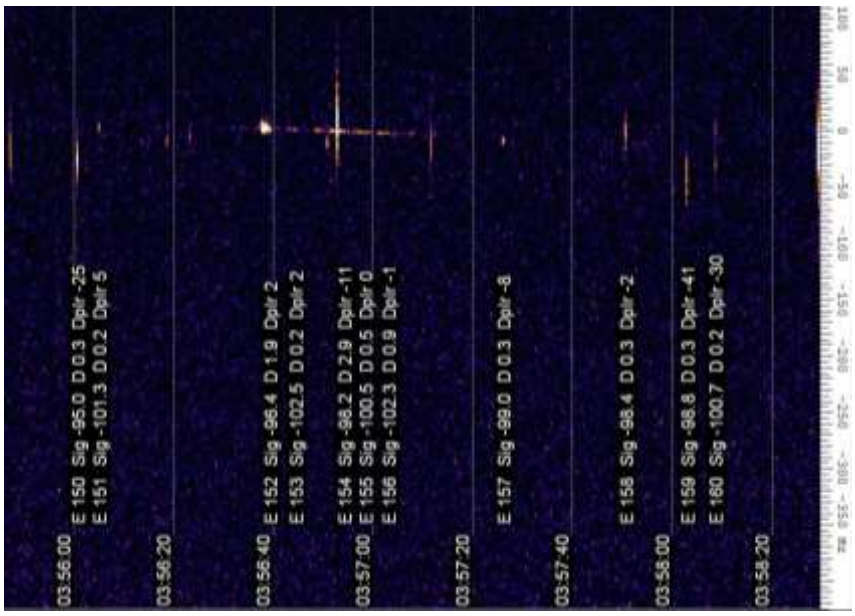

Fig 5 Including the Doppler shift on the printed screen information can help in distinguishing between genuine meteor events and interference.

Revised Conditional Actions script (MetScat_cleanseCA2v51.txt)

	If	Then	Remark
1	initialising	CenFreq=2512: PrntFreq=-250: TrigLvl=17	USER to set rx freq offset & screen freq for printing labels (both in Hz) and Trigger Level (dB above noise level)
2	initialising	TrigLo=(CenFreq-100): TrigHi=(CenFreq+100): NoiseLo=(CenFreq-200): NoiseHi=(CenFreq-100)	Calculate limits for Trigger and Noise bands
3	initialising	TrigDate= str("YYYY-MM-DD",time), TrigTime= str("hh:mm:ss"",time): Event=0:TrigSig=0: TrigNoise=0:TrigFreq=0: MDurn=0.0:Dplr=0	Define event_log registers at startup
4	initialising	R=0:S=0:E=0:	Clear STATE flags: R = System running; S = Signal present; E = Event in Progress
5	initialising	Sig=0:t1=0.0:t2=0.0: t3=0:t4=0:MCount=0: Trig=0:timer0.restart(2):timer3 .start(5)	Clear internal flags/registers and set start delays
6	always	h1=str("mmss",now)	to support end of hour reset of MCount/Event
7	timer3.expired(1)	R=1: sp.print("SYSTEM START")	Start system
8	new_spectrum	A=noise(NoiseLo,NoiseHi): Sig=peak_a(TrigLo,TrigHi: Trig=(A+TrigLvl)	Calculate new values after each FFT for trigger comparison
9	(R=1)&(Sig>Trig) &(E=1)&(S=1)	timer0.restart(2)	Case 1 - Continuing event
10	(R=1)&(Sig>Trig) &(E=1)&(S=0)	t1=time:S=1: timer0.restart(2)	Case 2 - Same event continuing after momentary break so register new start time
11	(R=1) &(Sig>Trig) &(E=0)	S=1:E=1: inc(MCount): t1=time: timer0.restart(2)	Case 3 - New event - record start time and initiate Timeout

	If	Then	Remark
12	continuation	Event=MCount: TrigTime= str("hh:mm:ss",time): TrigSig=Sig:TrigNoise=A: TrigFreq= peak_f(TrigLo,TrigHi): Dplr=int(TrigFreq- CenFreq+0.5)	Transfer trigger values to 'holding' registers
13	(R=1) &(Sig<=Trig) &(S=1)	t2=(timet1): MDurn=(MDurn+t2): S=0	Signal falls below trigger point so calculate duration and add to accumulator
14	(R=1)& (timer0.expired(1))	sp.print(f=PrntFreq, "E",Event," Sig",str("0.0",TrigSig), "D",str("#0.0",MDurn), "Dplr",Dplr:E=0:S=0	Event ended. Add Event#, Signal strength, Duration and Doppler shift to screen starting at position PrntFreq
15	Continuation	fopen2("c:\\Spectrum\\" +"event_log" +str("YYYYMMDD",now) +".txt",a)	Open Event Log file
16	continuation	fp2(TrigTime+","+Event+"," +str("0.0",TrigSig)+"," +str("0.0",TrigNoise)+"," +str("0000",TrigFreq)+"," +str("0.00",MDurn))	Save to file
17	continuation	fclose2: MDurn=0.0:t1=0.0:t2=0.0	Close event log and reset registers ready for next event
18	val(h1,"####") =5959	t3=0	Prepare to reset count
19	t3=0 & val(h1,"####") =0000	MCount=0:t3=t3+1	Events in progress at hour rollover will be numbered as previous hour

Announcement

Dear Radio Meteor Enthusiast,

You will be glad to know that following our BAA RAG Meteor Workshop presentation at Northampton Natural History Museum on 15th August 2015, Scatterthon was uploaded to an online repository hosting site called GitHub, on the 24 of December, 2015.

The application allows the classification of radio detections into meteor and non-meteor classes and outputs RMOB-format colorgrammes. This improves the quality of data collected by SpectrumLab scripts, published by Paul Hyde in BBC Sky at Night magazine.

Currently we are looking for a small group of testers to identify any remaining bugs in the application, in order that the application will be available as a stable version both for general download and open source development thereafter. If you'd be happy to join the test group, please let us know (email: *info@radioastro.org.uk*).

Please see below examples of current Scatterthon outputs for reference and visit the following links for more details regarding Meteor scatter, the Scatterthon application and our activities (please also note the software has developed since these presentations were given last August):

http://radio-space.co.uk/files/Links/JACKSON_Practical_Radio_Astronomy.pdf

http://radio-space.co.uk/files/Links/PENRICE_Scatterthon_Intro.pdf

Regards,

Chris and Victoria

info@radioastro.org.uk

07415094820

Scatterthon sample results

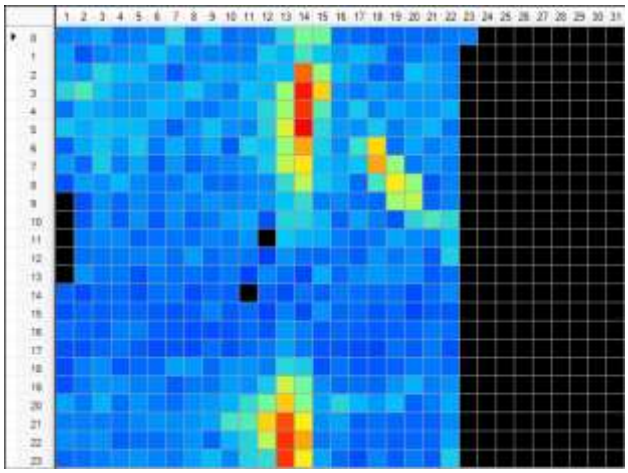

2014 12 Dec Geminids & moonbounce

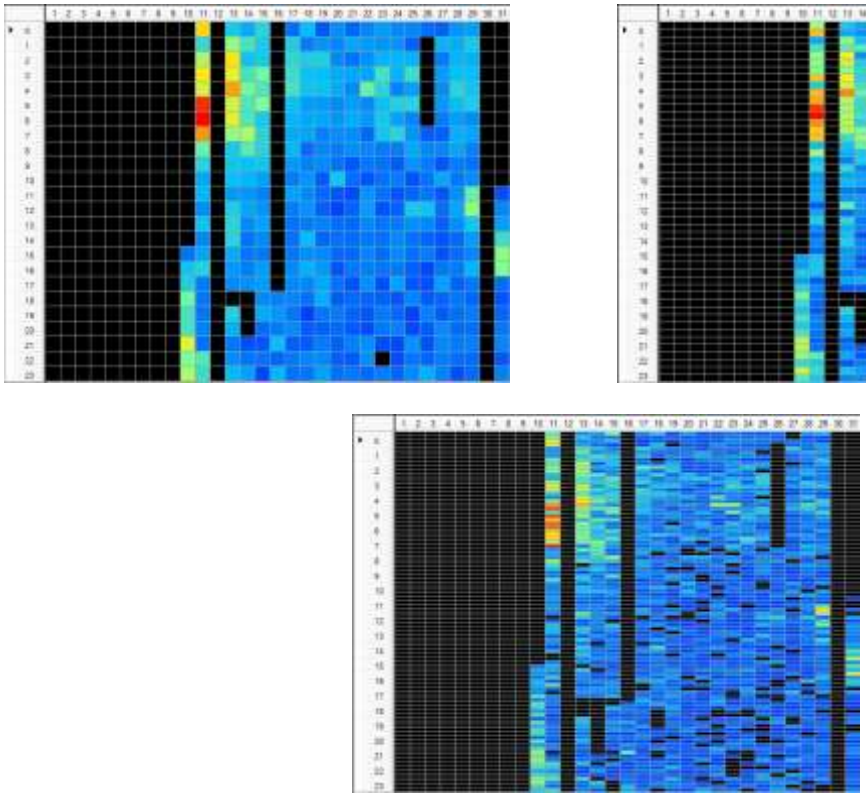

2014 08 Aug Perseids data at 60, 30 and 15-minute intervals

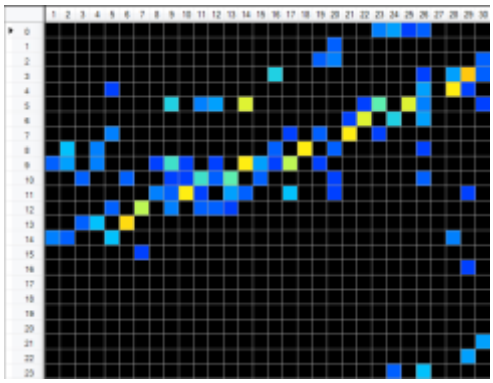

2014 11 Nov Classified Satellite activity, showing one particular satellite on a daily cycle, an hour earlier each day

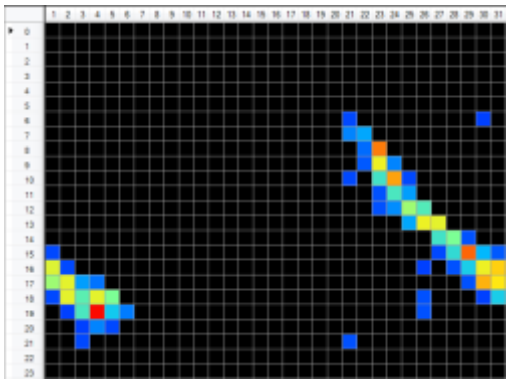

2014 10 Oct Classified Moon bounce signals, showing moon passage through the antenna's beam.